Coupling of Pressure-Induced Structural Shifts to Spectral Changes in a Yellow Fluorescent Protein

Buz Barstow,[‡] Nozomi Ando,[§] Chae Un Kim,[†] and Sol M. Gruner[†§*]
[†]Cornell High Energy Synchrotron Source, [‡]School of Applied Physics, and [§]Department of Physics, Cornell University, Ithaca, New York

ABSTRACT X-ray diffraction analysis of pressure-induced structural changes in the *Aequorea* yellow fluorescent protein Citrine reveals the structural basis for the continuous fluorescence peak shift from yellow to green that is observed on pressurization. This fluorescence peak shift is caused by a reorientation of the two elements of the Citrine chromophore. This study describes the structural linkages in Citrine that are responsible for the local reorientation of the chromophore. The deformation of the Citrine chromophore is actuated by the differential motion of two clusters of atoms that compose the β-barrel scaffold of the molecule, resulting in a slight bending of the β-barrel. The high-pressure structures also show a perturbation of the hydrogen bonding network that stabilizes the excited state of the Citrine chromophore. The perturbation of this network is implicated in the reduction of fluorescence intensity of Citrine. The blue-shift of the Citrine fluorescence spectrum resulting from the bending of the β-barrel provides structural insight into the transient blue-shifting of isolated yellow fluorescent protein molecules under ambient conditions and suggests mechanisms to alter the time-dependent behavior of Citrine under ambient conditions.

INTRODUCTION

It has long been appreciated that the three-dimensional structure of a protein molecule can exert a strong influence over the active site of the molecule (1). This linkage permits allosteric binding of ligands and processing of substrates. Examples of this include the R to T transition in hemoglobin (1), the allosteric inhibition of phosphofructokinase by phosphoenolpyruvate (2), and the gating of ion channels (3). Small structural changes, sometimes <1 Å in magnitude, in a distant part of the molecule may be communicated through the protein matrix to an active and/or binding site, promoting a change in binding constant, catalytic rate, or other functional change.

Although allosteric effects in protein molecules are the most common example of the coupling between the overall structure of a protein molecule and its active sites, they are not the only example of effects of this type. Protein atomic structures solved at pressures up to a few hundred MPa (4–13) indicate that atoms in protein molecules are typically displaced by $\approx$0.1–1 Å from their ambient pressure positions. Pressures in the same range also significantly modify protein function (14). For example, the flash decay rate of firefly luciferase is reduced (15), the R to T transition in human hemoglobin is biased (16) and oxidation rates by morphinone reductase are substantially increased (17). The results from these studies suggest that subtle changes in protein structure caused by pressure can have a profound effect on function. However, specific details on the exact linkages that are involved in the coupling of structure and function as a function of pressure have been lacking.

To systematically investigate the effect of pressure on protein structure and function, we studied the *Aequorea* yellow fluorescent protein (YFP) (18,19) variant, Citrine (20), using x-ray crystallography and fluorescence spectroscopy in the pressure range 0.1–5 MPa. In this case ''function'' is understood to refer to fluorescence. Citrine was chosen for this study as its bright intrinsic fluorescence could be readily assayed under conditions similar to that required by crystallography. We previously reported a direct correlation between a progressive subangstrom deformation of the Citrine chromophore and a corresponding change in the fluorescence spectrum of the molecule (13). In this study, we extend this work to describe how global structural changes in the larger protein matrix couple to the local deformation of the chromophore. Additionally, we report the pressure-induced structural changes that are responsible for a change in the fluorescence intensity.

The YFP family is distinguished from the *Aequorea* green fluorescent protein (GFP) family by the mutation T203Y. This mutation stacks a phenol ring $\approx$3.4 Å above the phenol ring of the wild-type main chromophore. The main chromophore is formed by the autocatalytic fusion of residues 65–67 and is referred to as residue 66. The weak interaction of the main chromophore and the phenol ring of Tyr^{203} is responsible for shifting the fluorescence peak of Citrine from green to yellow (18).

The majority of the Citrine scaffold is a β-barrel structure, approximately cylindrical with a diameter of $\approx$25 Å and a height of $\approx$50 Å (Fig. 1). Tyr^{203} forms part of the wall of the Citrine β-barrel, and its side chain, a phenol ring,

Submitted February 19, 2009, and accepted for publication June 24, 2009.

Nozomi Ando and Chae Un Kim contributed equally to this work.

*Correspondence: smg26@cornell.edu

Buz Barstow's present address is Department of Systems Biology, Harvard Medical School, Boston, MA 02115.

Nozomi Ando's present address is Department of Chemistry, Massachusetts Institute of Technology, Cambridge, MA 02139.

Editor: Enrico Gratton.

0006-3495/09/09/1719/9 $2.00

doi: 10.1016/j.bpj.2009.06.039

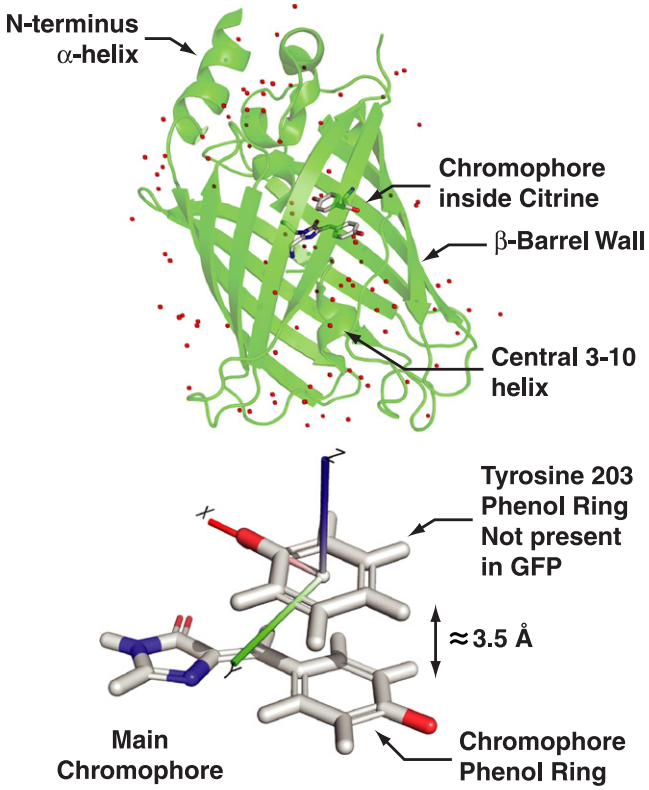

FIGURE 1 Ribbon diagram of the Citrine molecule and chromophore. The chromophore consists of the main chromophore and Tyr^{203}. The coordinate axes embedded in the Tyr^{203} phenol are used in the discussion in this article.

projects into the interior of the β-barrel. The main chromophore is attached to a 3-10 helix that threads through the center of the β-barrel. The top and bottom of the β-barrel consist of loops and the N-terminus α-helix.

We showed previously that the pressure-induced reorientation of the main chromophore and the Tyr^{203} phenol leads to a shift in the fluorescence peak of the Citrine from 527 nm at ambient pressure to 510 nm at pressures >350 MPa (13). As the pressure applied to Citrine is increased from ambient pressure to 500 MPa, the main chromophore moves continuously by $\approx$0.5 Å in the positive y-direction shown in Fig. 1 and $\approx$0.4 Å in the positive x-direction from its ambient pressure position relative to Tyr^{203}. This small deformation removes the perturbing influence of Tyr^{203} and permits the main chromophore to return to its green fluorescent state. An estimate of the effect of removing this perturbation on the fluorescence peak of Citrine is included in Section S1 of the Supporting Material.

To understand what global structural changes in the scaffold of Citrine are responsible for the local deformation observed at the chromophore, we analyzed the motion of individual residues as well as groups of residues in the crystal structures obtained at high pressure. The results of this analysis show that the chromophore motion is actuated by the concerted, differential motion of two groups of residues in the β-barrel wall and central 3-10 helix of the Citrine molecule. These results support the view that small global changes to the structure of a protein can be communicated to the active site and greatly affect its function. They also suggest that protein function may be modified by introducing mutations that affect the relative positions and motion of clusters of residues that may exist within a single domain of the protein.

EXPERIMENTAL PROCEDURES

Crystals of Citrine were grown as described previously (13). A closely spaced series of high-pressure structures of Citrine were solved using the high-pressure cryocooling x-ray crystallography technique developed by Kim et al. (8). Briefly, a protein crystal is pressurized with helium gas and is then cooled to 77 K, locking in collective pressure-induced structural changes (8,9). After pressure release, the protein molecules composing the crystal will retain many of the collective changes of the pressurized state, as long as the crystal temperature remains well below the protein glass transition temperature (9,14,21). Citrine crystals were prepared at pressures ranging from 50 to 500 MPa (13). Each structure at every pressure is derived from a different crystal at cryogenic temperatures. The high resolution limit of the datasets was typically <2 Å (13). The Citrine structures used in this analysis are listed in Table S1.

The fluorescence spectra of high-pressure cryocooled Citrine samples were recorded using a custom microspectrophotometer described previously (13). As the fluorescence spectra of YFPs are known to be sensitive to changes in solution pH (22), the choice of buffer was considered carefully. Citrine displayed a similar response to pressure under various buffers at room temperature (Section S2 of the Supporting Material), in agreement with reports that Citrine is less sensitive to changes in pH than other *Aequorea* YFPs (20). Nonetheless, buffers with low volume changes of ionization were selected to stabilize the pH for crystallization and spectroscopy (23,24).

To calculate the overall volume reduction of Citrine, the external surface and surfaces of internal cavities present in each solvent-stripped structure were identified and traced with the reduced surface computation program MSMS (25) using a 1.2 Å radius probe. The surfaces identified by MSMS were used to compute the volume enclosed by the external surface of each Citrine structure (the excluded volume) and the volumes of the cavities present in the interior of each Citrine structure. The net volume of each structure was computed by subtracting the total internal cavity volume from the excluded volume of the structure.

Clusters of residues that move in concert with increasing pressure in the series of Citrine atomic structures were identified using the heuristic clustering algorithm, RIGIMOL (DeLano Scientific LLC, Palo Alto, CA). Input coordinate files to RIGIMOL were prepared with PyMOL (DeLano Scientific LLC). Structural properties of Citrine atomic structures such as inertia tensors, centers of mass, and principal axes were computed using custom software implemented in PYTHON with use of the NUMPY numerical library. Fitting of structural parameters was carried out using the IPYTHON program and the NUMPY and SCIPY numerical libraries. Detailed discussion of the clustering algorithm and inertia tensor analysis can be found in Section S3 of the Supporting Material.

RESULTS

Nonisotropic volume reduction of Citrine under pressure

The deformation of Citrine due to pressure is very small in comparison to the overall dimension of the molecule. The

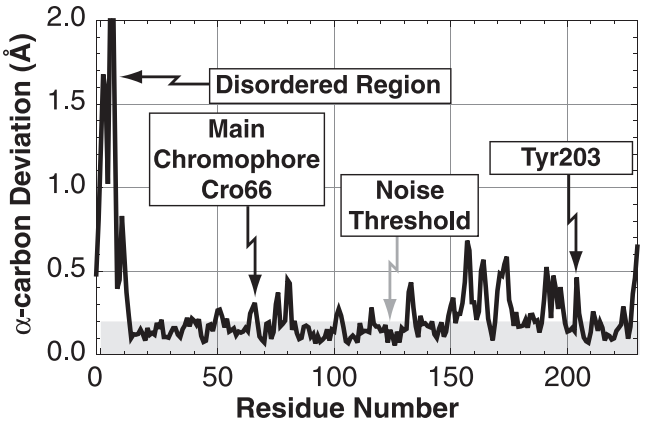

FIGURE 2 Average distance deviation between α-carbons of Citrine at 0.1 and 400 MPa versus residue number. Deviations below the gray band at 0.2 Å are at the uncertainty of the measurement.

superimposed structures of Citrine at 0.1 and 400 MPa are shown in Fig. S6. The overall volume of Citrine decreased by ~300 $Å^3$, or 1.1%, over the 500 MPa pressure range investigated (Section S4 and Fig. S7 of the Supporting Material), consistent with reported values of protein compressibility (26). The displacement of the α-carbons over this pressure range is small in magnitude when compared to the overall dimension of the protein. A plot of the average displacement of the α-carbon of each residue under a pressure increase from ambient pressure to 400 MPa is shown in Fig. 2. We estimate that the uncertainty in the displacements of the α-carbons is $\approx$0.2 Å, as indicated by the apparent ''noise threshold'' in Fig. 2 (9,11). In addition to the displacements seen at the disordered N-terminus of Citrine, there are numerous residues that were displaced by several times the noise threshold. Two notable displacements highlighted in Fig. 2 are the pressure-induced displacements of the main chromophore and Tyr^{203}, consistent with our previous report of the deformation of the chromophore (13). It is important to emphasize that although there are likely many residues in the structure of Citrine where the displacement due to pressurization is $<$0.2 Å, the positional uncertainties (27) on the Citrine structures do not permit the definitive identification of displacements smaller than the noise threshold (9,11) (Section S5 and Table S1 of the Supporting Material).

It is noted that the magnitudes of the residue displacements are nonuniform, suggesting the nonisotropic nature of the compression of Citrine, despite Citrine's overall linear volume reduction with pressure (Section S4 and Fig. S7 of the Supporting Material). Consistent with this, a distance difference matrix of the structures at 0.1 and 400 MPa show both the contraction and expansion of distances between residue pairs (Section S6 and Fig. S8 of the Supporting Material). If the compression of Citrine under high pressure were isotropic and homogeneous, we would expect that the relative orientation of the two elements of the chromophore would be retained with increasing pressure. However, the two chromophore elements slide apart with very little change in vertical separation with increasing pressure (13).

Principal axis and clustering analysis of Citrine compression

To further quantify the nonisotropic compression of Citrine, we analyzed the relative motion of clusters of atoms in the series of high-pressure Citrine structures. The β-barrel and the central 3-10 helix of Citrine were extracted from the series of high-pressure structures and aligned using the least squares fitting algorithm incorporated into PyMOL. The clustering algorithm RIGIMOL was used to identify clusters of atoms that move in concert with increased pressure. This analysis was restricted to the β-barrel and central 3-10 helix to avoid domination of the analysis by the disordered regions of the protein. The identification of clusters was found to be very reproducible, largely independent of choice of input structures (RIGIMOL can only take one structure per pressure as input), clustering algorithm parameters, and structural refinement method. (A description of the validation tests carried out on the RIGIMOL algorithm may be found in Section S3 of the Supporting Material.)

The clustering algorithm identified two clusters of atoms in the β-barrel and central 3-10 helix of Citrine that move with respect to one another as the pressure applied to the Citrine molecule is increased (Fig. 3). An important feature of the cluster assignment is that the perturbing Tyr^{203} is attached to cluster 1, whereas the main chromophore is attached to cluster 2. Over the investigated pressure range, the center of mass of cluster 1, containing the perturbing Tyr^{203} ring, moves by ≈ -0.2 Å in the x-direction with respect to that of cluster 2, which contains the main chromophore. For ease of reference, the coordinate axes used in this discussion are the same as those used by us in our prior work on the deformation of the chromophore of Citrine (13). This coordinate system is shown in Figs. 1 and 5. The cluster 1 center of mass appears to move relative to cluster 2 in the y-direction. However, this y-direction motion is small in comparison to the uncertainty on this motion, especially the displacement at 400 MPa. For this reason, it is difficult to discern if this motion is linear, perhaps extending to ≈ -0.05 Å by 500 MPa, or curved; returning to $\approx$0.0 Å at 500 MPa. There is no discernible motion in the z-direction.

Principal axis analysis shows that another component of the cluster movement is rotation. The principal axes of each cluster were found by computing the eigenvectors of the cluster's inertia tensor using the NUMPY numerical library. The principal axes were shown to rotate relative to one another by 1°–2° over 500 MPa (Figs. 4 and 5), suggesting a slight bending of the Citrine β-barrel wall. Consistent with this bending, principal axis analysis of the entire β-barrel wall suggests a redistribution of mass toward the side of the β-barrel wall containing Tyr^{203} (Section S7 of

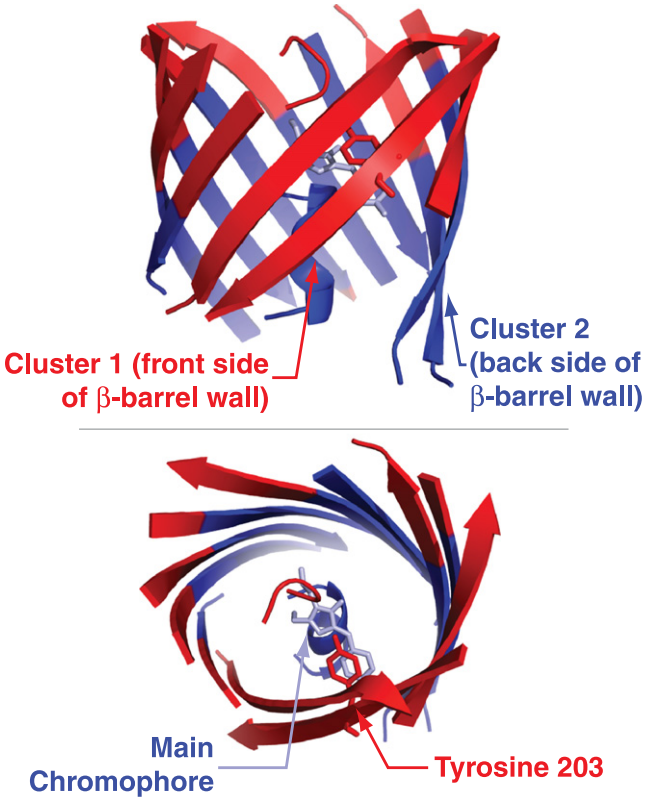

FIGURE 3 Clusters identified in the β-barrel walls and central 3-10 helix of the Citrine molecule that move in concert under high-pressure perturbation. Note that the main chromophore is attached to cluster 2, whereas the perturbing Tyr^{203} ring is attached to cluster 1. The main chromophore is colored light blue.

the Supporting Material). To investigate the effect of cluster motion on the chromophore, the pressure-induced translation and rotation of cluster 1 relative to cluster 2 were extracted and applied to Tyr^{203} of the ambient pressure structure, keeping the main chromophore fixed. Under these operations, Tyr^{203} moved in the negative x- and y-directions with respect to the main chromophore, consistent with the actual direction of movement observed at high pressure (13) (Fig. 5). This result suggests that the cluster translation, coupled with the slight rotation of the principal axes of the clusters, could possibly produce sufficient leverage to actuate the relative motion of the two elements of the Citrine chromophore.

Perturbation of hydrogen bonding network in chromophore cavity

We reported previously that the fluorescence peak of Citrine shifts to the blue with increasing pressure (13). Accompanying this blue-shift is a considerable reduction in fluorescence intensity, implying either a reduction in the quantum yield, a change in the absorption spectrum of Citrine, or both. The fluorescence peak intensity of Citrine solutions, high-pressure cryocooled at a range of pressures from 50 to 360 MPa, is shown in Fig. 6. The fluorescence peak intensity initially increases, from 0.1 MPa to 50 MPa, and then decreases. By a pressure of 200 MPa, the peak Citrine fluorescence intensity is $\approx$1/100th of its value at 50 MPa. Reports by Mauring et al. (28) and Ganesan et al. (29) suggest that the fluorescence intensity of Citrine may be modulated by the length of the hydrogen bond between the chromophore phenolic oxygen and the δ_1-nitrogen of His^{148}. The His^{148} δ_1-nitrogen to chromophore phenolic oxygen bond increases by 0.4 Å under a pressure increase from 0.1 to 500 MPa (Fig. 7).

In addition to the His^{148} δ_1-nitrogen to chromophore phenolic oxygen bond, the main chromophore is stabilized by several other hydrogen bonds. A simplified schematic of the hydrogen-bonding network stabilizing the Citrine

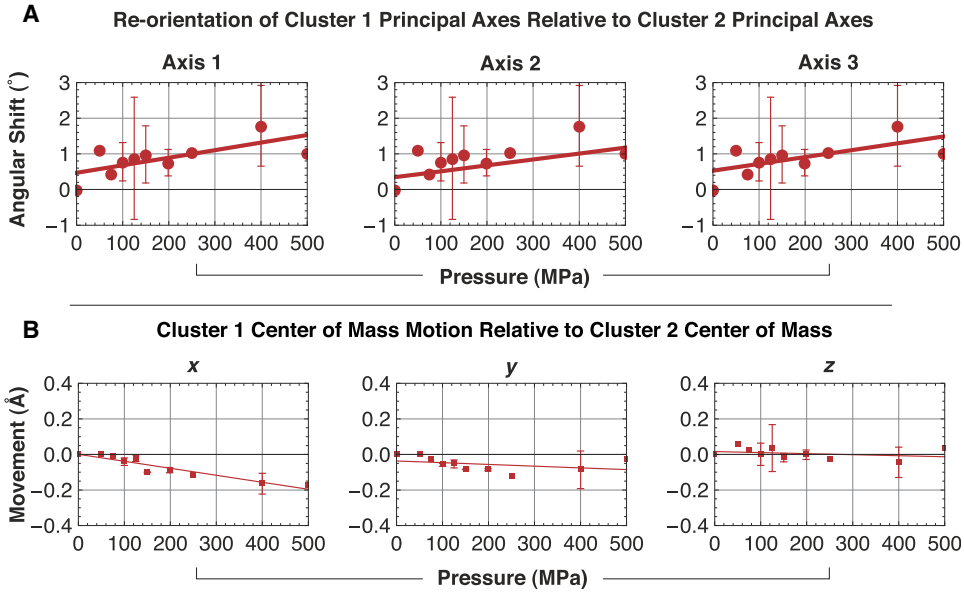

FIGURE 4 (*A*) Rotation of the principal axes of cluster 1 in a reference frame where the principal axes of cluster 2 are fixed. The angular shift is the angle formed between the principal axis at a given pressure and the principal axis at 0.1 MPa. (*B*) Motion of the center of mass of cluster 1 from its ambient pressure position in a reference frame where the cluster 2 center of mass is fixed. The directions of the coordinate axes of this system are shown in Figs. 1 and 5. Linear fit lines in all plots were determined by least squares fitting with the NUMPY numerical library. The fit lines are intended to help guide the eye and do not imply linear behavior.

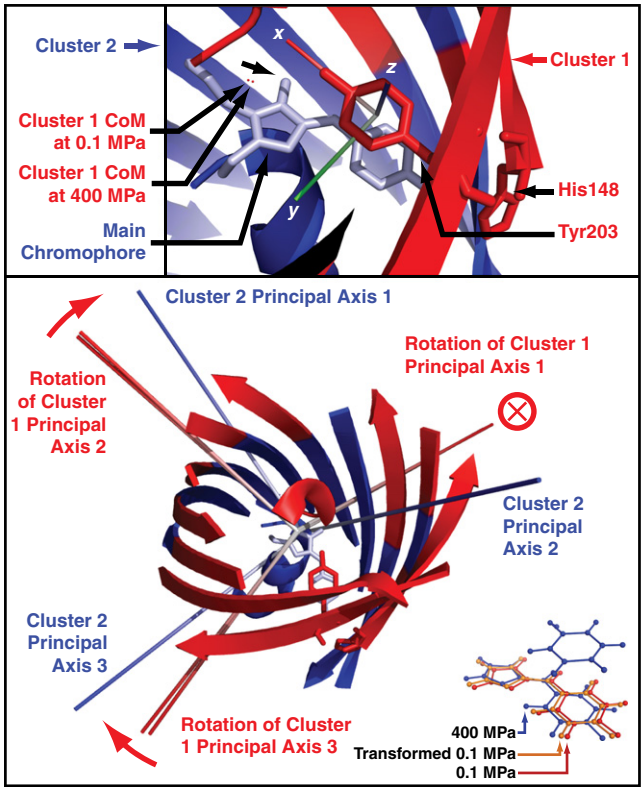

FIGURE 5 (*Upper panel*) Motion of the cluster 1 (*red*) center of mass in a reference frame where the center of mass of cluster 2 (*blue*) is fixed. (*Lower panel*) Rotation of cluster 1 principal axes relative to cluster 2 axes. The circled cross (⊗) next to cluster 1 principal axis 1 indicates that the rotation of the axis is into the figure. The main chromophore is colored in light blue for emphasis.

chromophore is shown in Fig. S10 *A*. Plots of behavior of other bonds in the chromophore cavity are shown in Fig. S10 *B*. A description of the behavior of the other bonds under pressure may be found in Section S8 of the Supporting Material.

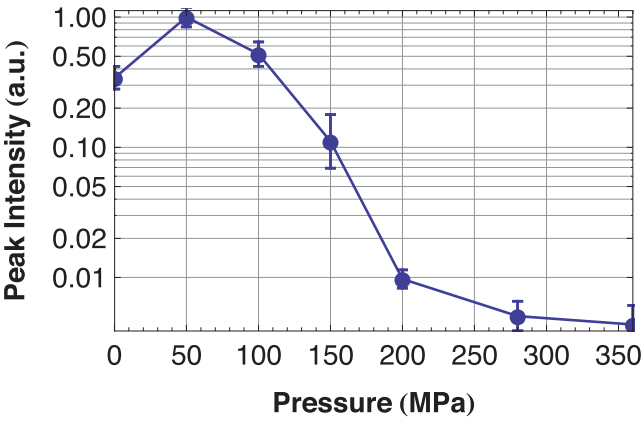

FIGURE 6 Fluorescence peak intensity of high-pressure cryo-cooled Citrine solution samples.

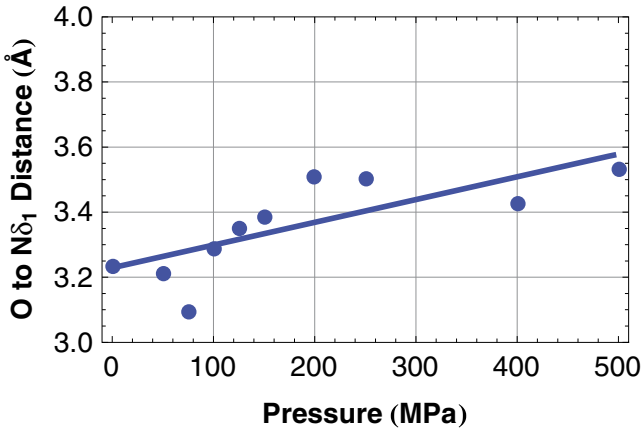

FIGURE 7 His^{148} δ_1-nitrogen to chromophore phenolic oxygen hydrogen bond length.

DISCUSSION

Reduction in fluorescence intensity with increasing pressure

Experiments on other *Aequorea* fluorescent protein (AFP) mutants suggest that the reduction in fluorescence intensity of Citrine under high-pressure cryocooling (Fig. 6) may be due to pressure-induced disruption of the chromophore cavity hydrogen-bonding network (18). This network serves to anchor the main chromophore, stabilizing the chromophore excited state, preventing nonradiative decay and facilitating the high quantum yield of the molecule (28). Niwa et al. (30) noted that certain analogs of the GFP chromophore (isolated from the β-barrel) absorb light yet are nonfluorescent at room temperature, but when frozen to cryogenic temperatures become fluorescent (30). Computer simulations indicate that in vacuum, the chromophore is fluorescent, whereas in liquid, the excited state of the molecule de-excites by quenching (31). Mauring et al. (28) showed that the application of high pressure to an *Aequorea* blue fluorescent protein (BFP) increased the quantum yield of the molecule. The central residue of the BFP chromophore is a histidine, a shorter residue than the tyrosine normally found at the center of an AFP chromophore. This shortened chromophore is unable to link to the chromophore cavity hydrogen-bonding network, leading to destabilization of the chromophore excited state. As a result, BFPs display lower quantum yields than other AFPs (28). Mauring et al. (28) attributed the pressure-induced increase in the quantum yield to the reattachment of the BFP chromophore to the chromophore cavity hydrogen-bonding network as the cavity was compressed.

Although the behavior of Citrine and EYFP (enhanced YFP) (32) under high pressure is the opposite of BFP (the fluorescence intensity reduces), the structural mechanism may be the same (perturbation of the chromophore cavity hydrogen-bonding network). The mutation H148V in YFP

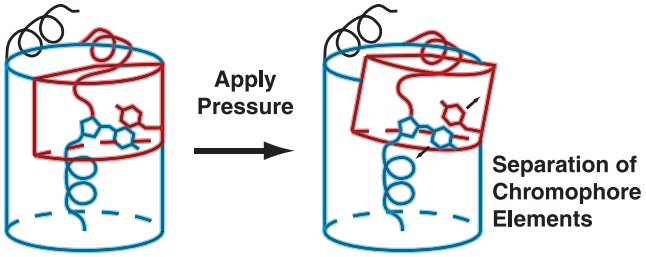

FIGURE 8 Cartoon representation of the bending of the Citrine scaffold.

removes a critical link in the hydrogen-bonding network attaching the phenolic oxygen of the main chromophore to the His^{148} δ_1-nitrogen and results in an 82% reduction in the fluorescence intensity with only a 15% drop in absorption (29). We speculate that the pressure-induced increase in this bond length is responsible for the reduction in fluorescence intensity of Citrine shown in Fig. 6.

Shifts in the absorption and fluorescence peaks of Citrine with increasing pressure at room temperature (Fig. S1) indicate that the Citrine absorption and fluorescence peaks maintain a constant Stokes shift. If this behavior is maintained at low temperature, then the absorption peak should blue-shift with increasing freezing pressure. As the high-pressure cryocooled Citrine solutions studied here were excited at 473 nm, the blue edge of Citrine absorption spectrum (the absorption peak at 0.1 MPa is 514 nm), we would expect absorption to increase with increasing freezing pressure. Thus, we speculate that the reduction in quantum yield of Citrine may be even greater than is implied by the reduction in fluorescence intensity seen in Fig. 6.

Deformation of the Citrine scaffold

The deformation of the Citrine scaffold can be thought of as the slight bending of the β-barrel scaffold. A cartoon representation of this deformation is shown in Fig. 8. As the pressure applied to the molecule is increased, the main chromophore remains anchored to cluster 2, attached to the central helix. However, the side of the β-barrel wall containing the perturbing Tyr^{203} ring and stabilizing His^{148} residue, moves away from cluster 2, carrying these two important residues with it. The large expansion of the distance from the central 3-10 helix to the wall of β-barrel in the vicinity of Tyr^{203} can be seen in the highlighted region in the distance difference matrix in Fig. S8.

It is interesting to note that the fluorescence peak intensity of all AFPs studied under pressure (13,32) increases with applied pressure, with the exception of the YFP types. The unusual pressure response of the YFPs at room temperature (32) and at cryogenic temperatures (13), may plausibly be due to a YFP structure that predisposes the YFP-type molecules to the bending behavior observed here.

There is no evidence that the crystalline environment significantly affects the fluorescence properties of the Citrine molecule relative to a solution of Citrine at equivalent concentration. The high optical density and overlapping absorption and fluorescence spectra of Citrine crystals, all of which had slightly different sizes, made it difficult to reproducibly measure the position of the peak of the fluorescence spectra of pressure cooled Citrine crystals. Thus, we were forced to seek a substitute: pressure cooled solutions in capillaries (13). The fluorescence spectra of a very small, flash frozen Citrine crystal and a flash frozen dilute solution of Citrine are plotted in Fig. S11 for comparison. The similarity of these two spectra suggests that the crystalline environment does not significantly perturb the fluorescence properties of Citrine. As pressure-induced unfolding is not expected to occur in the solution state of Citrine below at least 1000 MPa (33), it is plausible that the pressure effects captured in the crystalline state represents those in the solution state within the explored pressure range. This is reasonable as the deformation of Citrine in the crystal state is not a response to a directionally applied external force. As opposed to typical small molecule crystals, the fluid water channels intrinsic to most protein crystals constitute approximately half of the crystal mass and transmit hydrostatic pressure to each protein. A force originating at the surface of the crystal is not transmitted through covalent or metal bonds from molecule to molecule as happens in a small molecule crystal or a metal. There is no pressure gradient across the volume of the crystal: identical, uniform hydrostatic pressure is transmitted by the solvent channels to each molecule. Thus, the protein deformation in response to pressure is not due to an externally applied force per se; rather it results from pressure-dependent interactions of the molecule.

For example, it is known that the degree of ionization (34), hydration (34,35), and hydrogen bonding (34,36) of many amino acid residues are pressure dependent. It has also been shown that pressure changes the water occupancy of internal cavities (10,11,37,38). One expects that as these interactions change with pressure, the conformation of the protein will change in response. The fact that pressure is transmitted to the individual molecules in the crystal also argues that the resulting deformations are similar to those expected for the same molecule in solution, and differ only in so far as molecular contacts in the crystal change the surface exposure to water or constrain large deviations in protein structure. This belief is supported by earlier observation that both crystals and solutions of Citrine display the same release in the blue-shifting effects of pressure when warmed above the glass transition temperature and then recooled (13). This suggests that the structures of Citrine in the crystal and in solution do not diverge at elevated pressure. This contention is further supported by the similar response to pressure of the structure of hen egg-white lysozyme when measured by x-ray crystallography (6) and by high-pressure solution NMR (4).

At room temperature, the main chromophore of YFP protrudes slightly further, by $\approx$0.9 Å, into the chromophore

cavity than the chromophore in the EGFP structure (18). This preexisting deformation, possibly induced by the presence of the perturbing Tyr^{203} residue, may slightly weaken the YFP structure and predispose it to the bending behavior seen under high-pressure cryocooling. This bending behavior may be analogous to macroscopic structures failing at the weakest point.

Although the structure of Citrine and the response of its structure to high pressure are no doubt subtly different to that of wild-type GFP (wtGFP), the extension in path length from the phenolic oxygen to the ε_2-oxygen of Glu^{222} (Fig. S10) may also provide a framework for explaining the subtle pressure-induced red-shift in fluorescence peak of wtGFP (39). In the Citrine structures presented here, the distance from the phenolic oxygen of the main chromophore to the HOH-1 solvent molecule to the ε_2-oxygen of Glu^{222} increases by $\approx$0.5 Å from ambient pressure to 500 MPa. The increase in this distance should have no impact on the fluorescence properties of Citrine as excited state proton transfer from the main chromophore to Glu^{222} seems to play no role in the fluorescence mechanism of AFPs mutants containing phenolate anion chromophores (19). However, excited state proton transfer does play a role in the fluorescence mechanism of wtGFP, and the extension of the proton transfer path may be responsible for modification of the fluorescence properties of wtGFP under pressure (40,41).

An important observation from our earlier work (13) is that the fluorescence peak of Citrine approaches 510 nm, the fluorescence peak of EGFP under ambient conditions, as the pressure applied to the molecule is raised to >350 MPa. This shift to the green of the fluorescence peak is due to the removal of the perturbing effect of Tyr^{203} from the main chromophore (13). The results presented in this study, on the effect of high pressure on the scaffold of Citrine, indicate that the relative sliding motion of the Tyr^{203} phenol ring and the main chromophore is actuated by the separation of two clusters that compose the β-barrel wall and central 3-10 helix. This observation may provide a structural explanation for the observation of Blum et al. (42) that a single molecule of YFP (19,20) occasionally becomes dark, and then adopts a spectrum closely resembling the spectrum of bulk EGFP (19,43,44), before returning to a spectrum close to that of bulk YFP. It is known that many protein molecules fluctuate between a number of conformations (45). We speculate that at room temperature, YFPs may occasionally adopt a configuration structurally similar to the bent state seen at high-pressure. The bent scaffold of this state may transiently stabilize the main chromophore-Tyr^{203} separation needed for the molecule to fluoresce in the green. Single molecule experiments indicate that single enzymes display a range of catalytic rates (46,47), and switch between them, in much the same way that a single YFP molecule switches between several spectra (42). This result suggests that the high-pressure cryocooling technique may be useful for accessing the atomic structures of transiently populated enzyme states that are presently only observable in single molecule experiments. Experiments by Urayama et al. (9) indicated that high pressure stabilizes the structure of a room temperature conformational and functional substate of myoglobin. It is possible that the dark state of YFP observed by Blum et al. (42) is one in which the stabilizing interaction between the main chromophore and His^{148} is completely lost.

The structural information available on Citrine at high pressure may inspire structural modifications to Citrine that may permit the Citrine molecule to remain in the blue-shifted transient state for longer, or even permanently stabilize it. It may be possible to induce the bending of the Citrine scaffold seen at high-pressure under ambient conditions by repacking the Citrine scaffold by mutating or adding residues along the interface of these two clusters. On this basis, Fig. S12 shows several possible sites where one would logically seek to introduce mutations. To replicate the bending seen at high pressure, it is required that cluster 1 move down and to the right in the Fig. S12. It is interesting to consider if this may be achieved by simultaneously mutating residues on the left hand interface between clusters 1 and 2 to bulkier residues, and mutating those on the right hand interface to less bulky residues, while keeping other properties of the residues as similar as possible. On the left hand side, possible mutations may be Phe^{46} to Tyr or Trp, Val^{16} to Leu, Ile, or Met, Asn^{121} to Gln, Val^{112} to Leu, Ile, or Met, Tyr^{92} to Trp. On the right hand side, these mutations may be Ile^{161} to Val, Ala, or Gly, Gln^{183} to Asp, Cys, Thr, or Ser, Val^{163} to Ala or Gly, leaving Phe^{165} unchanged as it is the smallest aromatic amino acid. The success of this strategy would depend on the perturbations of these mutations being small enough to not affect the folding of the β-barrel scaffold. Although a blue-shifted YFP is of little practical value, it would be an important proof of principle. The same strategy may be applied to engineer new AFPs that can switch color in response to a trigger. Such a protein may be useful for single-molecule and imaging techniques. More significantly, if structural perturbations due to pressure of the character observed in Citrine are seen in catalytic proteins, it may be possible to introduce mutations similar to the ones suggested for Citrine to bias a population of catalytic molecules into more active conformations, resulting in an increase in the bulk rate of catalysis. Further discussion of this issue is included in Section S9.

CONCLUSIONS

We have shown that the scaffold of the Citrine molecule deforms under high-pressure. Rather than isotropically compressing, the high-pressure deformation of Citrine is nonhomogeneous. The Citrine β-barrel is approximately divided into two atomic clusters that move and rotate relative to one another under pressurization. The two elements of the Citrine chromophore, the perturbing Tyr^{203} ring and the main chromophore, are each attached to different clusters.

The relative motion and rotation of these two clusters causes a deformation in the Citrine scaffold that is reminiscent of bending, actuating the separation of the two elements of the Citrine chromophore, resulting in a fluorescence shift of the molecule. In addition to actuating the fluorescence shift of the molecule, the bending of the Citrine scaffold also perturbs the hydrogen-bonding network stabilizing the main chromophore. The most important consequence of this perturbation is an increase in the distance from the main chromophore phenol to the His^{148} side chain. The increase in the His^{148} to main chromophore distance may plausibly result in a destabilization of the excited state of the chromophore and the consequent dimming of Citrine seen under high-pressure cryocooling conditions (13) and under high hydrostatic pressure (32).

The bent state of the Citrine scaffold may be highly structurally similar to the transiently observed blue-shifted state of YFP at ambient pressure (42). This suggests that high-pressure x-ray crystallography may offer the possibility of solving the structures of transiently occupied enzymatic states and understanding the structural basis of their differing catalytic rates. These high-pressure structures of Citrine may inspire mutations that permit Citrine to remain in the blue-shifted state for longer periods of time.

Finally, these experiments explicitly demonstrate the continuous linkage of a protein scaffold and activity (fluorescence in this case) of the protein. Studies of the effects of pressure on the structure and function of protein molecules yield several insights into the structure-function relationship of these molecules. First, these studies probe the energy landscapes of protein active sites and offer what we believe is new insight on the structural basis of enzymatic catalysis. Second, these studies illustrate the coupling of protein active sites and the protein matrix, giving additional insights into the structural basis of allosteric behavior, especially in monomeric proteins. Third, these experiments may provide structural explanation of the results of single molecule experiments, by allowing the trapping of normally transiently occupied protein states, as we believe was shown with Citrine. Fourth, these studies may highlight the tunability of protein, especially enzymatic activity, and suggest avenues for improving the function of protein molecules under ambient conditions that may not be highlighted by single protein structures, random mutagenesis, or directed evolution methods.

SUPPORTING MATERIAL

Nine sections, a table, and 12 figures are available at http://www.biophysj.org/biophysj/supplemental/S0006-3495(09)01215-6.

The authors thank Dr. Cynthia Kinsland and the staff of the Cornell Life Sciences Core Lab Centers Protein Facility for assistance with the modification and expression of Citrine vectors, and protein purification and the MacCHESS staff at the Cornell High Energy Synchrotron Source (CHESS) for assistance in data collection and reduction (MacCHESS is the macromolecular division of CHESS). We thank Martin Novak for invaluable assistance with the construction of experiments, Yi-Fan Chen and Dr. Mark Tate (Cornell University) for the construction of the internals of the high pressure cryocooling apparatus, Odin Wojcik and AccuFab Inc. (Ithaca, NY) for the construction of the high pressure cryocooling safety enclosure, Professor Warren Zipfel (Cornell University) for providing a sample of monomeric EGFP, Professor Roger Tsien (University of California, San Diego) for providing the Citrine plasmid, Dr. Gerhard Hummer (National Institute of Diabetes and Digestive and Kidney Diseases), Dr. Ismail Hafez (University of British Columbia, Vancouver), Professors Lois Pollack and Brian Crane (Cornell University) for useful discussions, Professor Robert Campbell (University of Alberta) for assistance with crystallization of Citrine, Elizabeth Landrum and Darren Southworth for assistance in data collection and Joan Lenz and Dr. Raymond Molloy (Cornell University) for assistance with molecular biology.

This work is supported by the Department of Energy/ Biological and Environmental Research (FG02-97ER62443), and National Institutes of Health Protein Structure Initiative (GM074899). CHESS is supported by the National Science Foundation and National Institutes of Health via National Science Foundation award DMR-0225180, and MacCHESS is supported via National Institutes of Health grant RR001646.

REFERENCES

1. Perutz, M. F., G. Fermi, B. Luisi, B. Shaanan, and R. C. Liddington. 1987. Stereochemistry of cooperative mechanisms in hemoglobin. *Acc. Chem. Res.* 20:309–321.
2. Schirmer, T., and P. R. Evans. 1990. Structural basis of the allosteric behavior of phosphofructokinase. *Nature*. 343:140–145.
3. Long, S. B., X. Tao, E. B. Campbell, and R. Mackinnon. 2007. Atomic structure of a voltage-dependent K^+ channel in a lipid membrane-like environment. *Nature*. 450:376–382.
4. Refaee, M., T. Tezuka, K. Akasaka, and M. P. Williamson. 2003. Pressure-dependent changes in the solution structure of hen egg-white lysozyme. *J. Mol. Biol.* 327:857–865.
5. Fourme, R., E. Girard, R. Kahn, I. Ascone, M. Mezouar, et al. 2003. Using a quasi-parallel x-ray beam of ultrashort wavelength for high-pressure virus crystallography: implications for standard macromolecular crystallography. *Acta Crystallogr. D Biol. Crystallogr.* 59:1767–1772.
6. Kundrot, C., and F. Richards. 1987. Crystal structure of hen egg-white lysozyme at a hydrostatic pressure of 1000 atmospheres. *J. Mol. Biol.* 193:157–170.
7. Kundrot, C., and F. Richards. 1986. Collection and processing of x–ray diffraction data from protein crystals at high pressure. *J. Appl. Cryst.* 19:208–213.
8. Kim, C. U., R. Kapfer, and S. M. Gruner. 2005. High-pressure cooling of protein crystals without cryoprotectants. *Acta Crystallogr. D Biol. Crystallogr.* 61:881–890.
9. Urayama, P. K., G. N. Phillips, and S. M. Gruner. 2002. Probing substates in sperm whale myoglobin using high-pressure crystallography. *Structure*. 10:51–60.
10. Collins, M. D., G. Hummer, M. L. Quillin, B. W. Matthews, and S. M. Gruner. 2005. Cooperative water filling of a nonpolar protein cavity observed by high-pressure crystallography and simulation. *Proc. Natl. Acad. Sci. USA*. 102:16668–16671.
11. Collins, M. D., M. L. Quillin, G. Hummer, B. W. Matthews, and S. M. Gruner. 2007. Structural rigidity of a large cavity-containing protein revealed by high-pressure crystallography. *J. Mol. Biol.* 367:752–763.
12. Williamson, M. P., K. Akasaka, and M. Refaee. 2003. The solution structure of bovine pancreatic trypsin inhibitor at high pressure. *Protein Sci.* 12:1971–1979.
13. Barstow, B., N. Ando, C. U. Kim, and S. M. Gruner. 2008. Alteration of citrine structure by hydrostatic pressure explains the accompanying spectral shift. *Proc. Natl. Acad. Sci. USA*. 105:13362–13366.
14. Frauenfelder, H., N. A. Alberding, A. Ansari, D. Braunstein, B. R. Cowen, et al. 1990. Proteins and pressure. *J. Phys. Chem.* 94:1024–1037.

15. Ueda, I., H. Minami, H. Matsuki, and T. Inoue. 1999. Does pressure antagonize anesthesia? High-pressure stopped-flow study of firefly luciferase and anatomy of initial flash. *Biophys. J.* 76:478–482.

16. Unno, M., K. Ishimori, and I. Morishima. 1990. High-pressure laser photolysis study of hemoproteins. Effects of pressure on carbon monoxide binding dynamics for R- and T-state hemoglobins. *Biochemistry.* 29:10199–10205.

17. Hay, S., M. J. Sutcliffe, and N. S. Scrutton. 2007. Promoting motions in enzyme catalysis probed by pressure studies of kinetic isotope effects. *Proc. Natl. Acad. Sci. USA.* 104:507–512.

18. Wachter, R. M., M. Elsliger, K. Kallio, G. T. Hanson, and S. J. Remington. 1998. Structural basis of spectral shifts in the yellow-emission variants of green fluorescent protein. *Structure.* 6:1267–1277.

19. Tsien, R. Y. 1998. The green fluorescent protein. *Annu. Rev. Biochem.* 67:509–544.

20. Griesbeck, O., G. S. Baird, R. E. Campbell, D. A. Zacharias, and R. Y. Tsien. 2001. Reducing the environmental sensitivity of yellow fluorescent protein. Mechanism and applications. *J. Biol. Chem.* 276:29188–29194.

21. Kim, C. U., Y. Chen, M. W. Tate, and S. M. Gruner. 2007. Pressure induced high-density amorphous ice in protein crystals. *J. Appl. Cryst.* 41:1–7.

22. Elsliger, M. A., R. M. Wachter, G. T. Hanson, K. Kallio, and S. J. Remington. 1999. Structural and spectral response of green fluorescent protein variants to changes in pH. *Biochemistry.* 38:5296–5301.

23. Neuman, R., W. Kauzmann, and A. Zipp. 1973. Pressure dependence of weak acid ionization in aqueous buffers. *J. Phys. Chem.* 77:2687–2691.

24. Zipp, A., and W. Kauzmann. 1973. Pressure denaturation of metmyoglobin. *Biochemistry.* 12:4217–4228.

25. Sanner, M. F., A. J. Olson, and J. C. Spehner. 1996. Reduced surface: an efficient way to compute molecular surfaces. *Biopolymers.* 38:305–320.

26. Heremans, K., and L. Smeller. 1998. Protein structure and dynamics at high pressure. *Biochim. Biophys. Acta.* 1386:353–370.

27. Cruickshank, D. 1999. Remarks about protein structure precision. *Acta Crystallogr. D Biol. Crystallogr.* 55:583–601.

28. Mauring, K., J. Deich, F. I. Rosell, T. B. McAnaney, W. E. Moerner, et al. 2005. Enhancement of the fluorescence of the blue fluorescent proteins by high pressure or low temperature. *J. Phys. Chem. B.* 109:12976–12981.

29. Ganesan, S., S. M. Ameer-Beg, T. T. Ng, B. Vojnovic, and F. S. Wouters. 2006. A dark yellow fluorescent protein (YFP)-based resonance energy-accepting chromoprotein (REACh) for Forster resonance energy transfer with GFP. *Proc. Natl. Acad. Sci. USA.* 103:4089–4094.

30. Niwa, H., S. Inouye, T. Hirano, T. Matsuno, S. Kojima, et al. 1996. Chemical nature of the light emitter of the Aequorea green fluorescent protein. *Proc. Natl. Acad. Sci. USA.* 93:13617–13622.

31. Toniolo, A., S. Olsen, L. Manohar, and T. Martínez. 2004. Conical intersection dynamics in solution: the chromophore of green fluorescent protein. *Faraday Discuss.* 127:149–163.

32. Verkhusha, V. V., A. E. Pozhitkov, S. A. Smirnov, J. W. Borst, A. van Hoek, et al. 2003. Effect of high pressure and reversed micelles on the fluorescent proteins. *Biochim. Biophys. Acta.* 1622:192–195.

33. Scheyhing, C. H., F. Meersman, M. A. Ehrmann, K. Heremans, and R. F. Vogel. 2002. Temperature-pressure stability of green fluorescent protein: a Fourier transform infrared spectroscopy study. *Biopolymers.* 65:244–253.

34. Mozhaev, V., K. Heremans, J. Frank, P. Masson, and C. Balny. 1996. High pressure effects on protein structure and function. *Proteins.* 24:81–91.

35. Gross, M., and R. Jaenicke. 1994. Proteins under pressure. The influence of high hydrostatic pressure on structure, function and assembly of proteins and protein complexes. *Eur. J. Biochem.* 221:617–630.

36. Le Tilly, V., O. Sire, B. Alpert, and P. T. Wong. 1992. An infrared study of 2H-bond variation in myoglobin revealed by high pressure. *Eur. J. Biochem.* 205:1061–1065.

37. Ando, N., B. Barstow, W. A. Baase, A. Fields, B. W. Matthews, et al. 2008. Structural and thermodynamic characterization of T4 lysozyme mutants and the contribution of internal cavities to pressure denaturation. *Biochemistry.* 47:11097–11109.

38. Hummer, G., S. Garde, A. E. García, M. E. Paulaitis, and L. R. Pratt. 1998. The pressure dependence of hydrophobic interactions is consistent with the observed pressure denaturation of proteins. *Proc. Natl. Acad. Sci. USA.* 95:1552–1555.

39. Oger, P. M., I. Daniel, and A. Picard. 2006. Development of a low-pressure diamond anvil cell and analytical tools to monitor microbial activities in situ under controlled P and T. *Biochim. Biophys. Acta.* 1764:434–442.

40. Leiderman, P., R. Gepshtein, I. Tsimberov, and D. Huppert. 2008. Effect of temperature on excited-state proton tunneling in wt-green fluorescent protein. *J. Phys. Chem. B.* 112:1232–1239.

41. Lill, M. A., and V. Helms. 2002. Proton shuttle in green fluorescent protein studied by dynamic simulations. *Proc. Natl. Acad. Sci. USA.* 99:2778–2781.

42. Blum, C., A. J. Meixner, and V. Subramaniam. 2004. Room temperature spectrally resolved single-molecule spectroscopy reveals new spectral forms and photophysical versatility of *Aequorea* green fluorescent protein variants. *Biophys. J.* 87:4172–4179.

43. Cubitt, A. B., R. Heim, S. R. Adams, A. E. Boyd, L. A. Gross, et al. 1995. Understanding, improving and using green fluorescent proteins. *Trends Biochem. Sci.* 20:448–455.

44. Brejc, K., T. K. Sixma, P. A. Kitts, S. R. Kain, R. Y. Tsien, et al. 1997. Structural basis for dual excitation and photoisomerization of the Aequorea victoria green fluorescent protein. *Proc. Natl. Acad. Sci. USA.* 94:2306–2311.

45. English, B., W. Min, A. Van Oijen, K. Lee, G. Luo, et al. 2006. Ever-fluctuating single enzyme molecules: Michaelis-Menten equation revisited. *Nat. Chem. Biol.* 2:87–94.

46. Min, W., B. P. English, G. Luo, B. J. Cherayil, S. C. Kou, et al. 2005. Fluctuating enzymes: lessons from single-molecule studies. *Acc. Chem. Res.* 38:923–931.

47. Kou, S., B. Cherayil, W. Min, B. English, and X. Xie. 2005. Single-molecule Michaelis-Menten equations. *J. Phys. Chem. B.* 109:19068–19081.

Biophysical Journal, Volume 97

Supporting Material

Coupling of Pressure-Induced Structural Shifts to Spectral Changes in a Yellow Fluorescent Protein

Buz Barstow, Nozomi Ando, Chae Un Kim, and Sol M. Gruner

Supporting Online Material For:

Coupling of Pressure-Induced Structural Shifts to Spectral Changes in a Yellow Fluorescent Protein

Buz Barstow [†¶], *Nozomi Ando* [‡||], *Chae Un Kim* [§] *and Sol M. Gruner* [§||]

Present Address: [†] *Department of Systems Biology, Harvard Medical School, Boston, MA 02115, USA*

Present Address: [‡] *Department of Chemistry, Massachusetts Institute of Technology, Cambridge, MA 02139, USA*

[§] *Cornell High Energy Synchrotron Source,* [¶] *School of Applied Physics,* [||] *Department of Physics, Cornell University, Ithaca, NY 14853, USA*

Corresponding Author: Sol M. Gruner

Email: smg26@cornell.edu

Telephone: 607-255-3441

S1. Calculation of Fluorescence Peak Shift

To gain an intuitive understanding of the spectral shift of Citrine's fluorescence peak at high-pressure, a simple computer model of Citrine's energy levels was constructed using the Extended Hückel Theory (EHT) codes CACAO (1) and YAEHMOP (http://yaehmop.sourceforge.net). CACAO and YAEHMOP both perform identical calculations. CACAO is known to suffer from a number of bugs but has superior graphical presentation abilities to YAEHMOP. Simulations were performed using both programs and the results were compared. Identical results were obtained in all cases presented here.

Extended Hückel Theory (EHT) is one of the simplest formulations for computing the quantum mechanical wavefunctions of molecules (2). For a complete description of the theory, the reader should refer to the recent review of quantum chemical modeling techniques by Cramer (2). The theory often correctly identifies trends in molecular properties given perturbations to the geometry of the molecule (3).

Justification For Use of Extended Hückel Theory

Several observations indicate that it may be justified to use a simple Extended Hückel Theory model describe the shift in the fluorescence peak of Citrine with high pressure. Most importantly, at least at room temperature, the fluorescence and absorption peaks of Citrine move together as the pressure applied to the molecule is increased. This suggests that arguments about the energy landscape of Citrine that might normally be applied only to the absorption spectrum may also be applied to the fluorescence spectrum. The absorption and emission peaks of Citrine at room temperature are shown as a function of pressure in fig. S1. In addition, the Citrine fluorescence lifetime is very short, ≈ 3.6 ns (4), and the absorption and emission spectra of the molecule are symmetrical about their overlap point. Thus, it is reasonable to believe that a simple Franck-Condon model of fluorescence may reasonably describe the fluorescence mechanism of Citrine (5). This model is described in detail in chapter 1 of the text by Lakowicz (5). In this model the absorption and fluorescence of light is due to the radiative transitions of electrons between the vibrational substates of two electronic energy levels of a chromophore: usually the highest occupied molecular orbital (HOMO) and lowest unoccupied molecular orbital (LUMO). The Stokes shift of the fluorescence, the red-shift of the fluorescence peak when compared with the absorption peak, is due to non-radiative energy loss by the electrons involved in absorption and fluorescence due to transitions between the vibrational substates of the HOMO and LUMO.

X-ray crystallographic structures of protein molecules under high pressure (6-12) indicate that pressures up to a few hundred MPa do not significantly alter covalent bond lengths in protein molecules. Additionally, experiments by Isaacs *et al*. (13) suggest pressures in the same range will also not appreciably alter the vibrational frequencies of the atoms in the Citrine chromophore. Thus, it is not unreasonable to believe that the energy spacing of the vibrational energy levels of the Citrine chromophore will be unaffected by the application of pressures up to a few hundred MPa. For these reasons, it is plausible that the fluorescence peak shift of the Citrine molecule under high pressure may be due to the variation of the energy band-gap between the ground state of the chromophore, the HOMO, and the first excited state of the chromophore: the LUMO.

This may allow an extended Hückel calculation of the HOMO-LUMO band-gap to be used to semi-quantitatively explain the fluorescence shift of the Citrine molecule under high pressure in terms of the deformation of the Citrine chromophore structure by high pressure.

Results of Extended Hückel Simulations of Fluorescence Peak Shift of Citrine

We used truncated versions of the high-pressure structures of the Citrine chromophore (table S1) as inputs to the YAEHMOP code, and calculated the corresponding band-gap between the highest occupied molecular orbital (HOMO) and lowest unoccupied molecular orbital (LUMO) of the chromophore. The truncated chromophore input into the YAEHMOP code is shown in fig. S2.

The results of the extended Hückel computation are shown in fig. S3. Fig. S3 shows the measured and average calculated shift in energy of the fluorescence peak from its value at ambient pressure. The value of the measured fluorescence band-gap shift at 500 MPa was taken as that of mEGFP relative to Citrine at 0.1 MPa at ≈ 100 K (500 nm versus 527 nm) (12). We consider this to be a reasonable estimate of the upper value of the fluorescence band-gap shift.

The calculated shifts shown in fig. S3, $\Delta E_{\mathrm{c}}(P)$, from the ambient pressure HOMO-LUMO band-gap are compared with the measured energy shifts at each pressure,

$$\Delta E_{\mathrm{c}}(P) = E_{\mathrm{c}}(P) - E_{\mathrm{c}}(P_0). \tag{S1.1}$$

For the measured fluorescence band-gap, the energy shift from ambient pressure, ΔE_{m}, was calculated from the fluorescence wavelength data shown our earlier work on Citrine (12),

$$\Delta E_{\mathrm{m}}(P) = hc\left(\frac{1}{\lambda_{\mathrm{m}}(P)} - \frac{1}{\lambda_{\mathrm{m}}(P_0)}\right), \tag{S1.2}$$

where P_0 is 0.1 MPa.

The measured and calculated fluorescence band-gap shifts, $\Delta E_{\mathrm{m}}(P)$ and $\Delta E_{\mathrm{c}}(P)$ respectively, are presented in terms of energy, rather than wavelength as the measured and calculated baseline energies and wavelengths are different. We believe that it is unreasonable to expect this simple extended Hückel model of the Citrine fluorescence spectrum to correctly calculate the baseline HOMO-LUMO band-gap given the limited structure input into the model, and that much more sophisticated quantum chemical methodologies appear necessary to accurately estimate the fluorescence peak of the *Aequorea* fluorescent proteins (14). However, we do believe it reasonable to expect that this simple perturbation model could accurately calculate deviations from this baseline energy. However, if the results of this perturbation calculation were presented in term of wavelength, the calculated shift would appear inaccurate due to differences in baseline energies. To illustrate

$$\begin{aligned}\Delta\lambda(P) &= \lambda(P) - \lambda(P_0)\\ \Delta\lambda(P) &= \frac{hc}{E_0 - \Delta E} - \frac{hc}{E_0}\\ \Delta\lambda(P) &= \frac{hc}{E_0^2}\left(\frac{E_0 - E_0 + \Delta E}{1 - \Delta E/E_0}\right)\cdot\\ \Delta\lambda(P) &= \frac{hc\Delta E}{E_0^2}\left(1 - \Delta E/E_0\right)^{-1}\end{aligned} \tag{S1.3}$$

Binomially expanding the inverse term,

$$\Delta\lambda(P) = \frac{hc\Delta E}{E_0^2}\left(1 + \Delta E/E_0 + \ldots\right). \tag{S1.4}$$

As $\Delta E/E_0$ is on the order of 1/100th for wavelength shifts of several nanometers from baseline wavelengths of several hundred nanometers,

$$\Delta\lambda(P) \approx \frac{hc\Delta E(P)}{E_0^2}. \tag{S1.5}$$

Thus, as wavelength shifts are scaled by the inverse square of the baseline energy, comparison of two energy shifts from differing baseline energies can be misleading. The comparison of energy shifts, while less intuitive for an optical phenomenon such as a shift in fluorescence peak, is unambiguous.

Errors on the calculated fluorescence energy band-gap were estimated by a Monte Carlo procedure in which the main chromophore was randomly translated and rotated inside the error volume allowed by Cruickshank's positional uncertainty formula (15). Translations and rotations were performed with the PyMOL molecular graphics and manipulation program (DeLano Scientific LLC, Palo Alto, CA, USA). For the simulation results presented in fig. S3, 1000 random simulated perturbations were generated for each high-pressure structure. The HOMO-LUMO energy gap was calculated for each slightly perturbed structure with the extended Hückel theory program YAEHMOP. The highest and lowest energy band-gaps calculated in this procedure were recorded and taken as estimates upper and lower limits on the HOMO-LUMO band-gap for each high pressure Citrine structure, given the estimated positional uncertainty on the structure.

The calculated data points shown in fig. S3 are the average of the calculated HOMO-LUMO band-gaps for the unperturbed structures at each pressure. The error bars shown in fig. S3 correspond to the average highest and lowest values of the energy band-gap calculated during this random translation and rotation procedure at each pressure.

The baseline energy of the simulated band-gaps, was taken as the value of the energy band-gap of structure citrine0001_2 (PDB accession code 3DPW).

In general, the extended Hückel theory procedure finds reasonable agreement between the measured and calculated shifts in the fluorescence band-gap. This result suggests that the

mechanism of the fluorescence peak shift of Citrine under high-pressure cryocooling is the removal of the overlap of the orbitals of the tyrosine 203 phenol from the orbitals of the main chromophore. The result also supports the observed structural deformation of Citrine under high-pressure, suggesting that the deformation motion is real, rather than an artifact of refinement and data collection.

However, it is important to stress that the simple Extended Hückel model of the Citrine fluorescence peak shift is not the final word on the quantum mechanical mechanism of the Citrine fluorescence peak shift due to limitations of EHT.

Firstly, as we have noted before, the EHT model of the Citrine chromophore does not accurately calculate the Citrine fluorescence band-gap energy. At ambient pressure, the calculated fluorescence band-gap corresponds to a wavelength of ≈ 643 nm, while the observed fluorescence peak is 527 nm. As the errors on the calculated peak shift are comparable in magnitude to the peak shift (fig. S3), it is difficult to confirm the accuracy of the calculation. Additionally, it is difficult to confirm if the model produces the correct results for the right reasons.

The discrepancy between the calculated and observed ambient pressure fluorescence band-gap may in part be due to the limited structure input into EHT model of Citrine's fluorescence spectrum. However, the Citrine scaffold is believed to not significantly tune the absorbance of the chromophore (16). This suggests that the discrepancy in calculated and observed band-gaps is largely due to limitations intrinsic to EHT. Most importantly, EHT does not calculate the effects of electron-electron interaction. This limitation is particularly serious, as it does not permit calculation of changes in energy levels due to photo-excitation of the chromophore. This limitation also excludes the possibility of identifying small conformational changes to the chromophore upon photo-excitation.

More sophisticated methodologies have been applied to the fluorescence spectrum of the Green Fluorescent Protein chromophore. Toniolo *et al*. (16) used a combined semi-empirical quantum mechanical/molecular mechanical (QM/MM) simulation to explore the effects of solvation on the fluorescence lifetime of the chromophore. Toniolo *et al*. (16) found that solvation reduced the fluorescence lifetime of the chromophore by more than an order of magnitude, explaining the reduced quantum yield of GFP chromophore analogs in solution (17). These simulations suggested that rotation of the chromophore phenol ring relative to the imidazolinone ring was responsible for non-radiative de-excitation of the chromophore.

Sinicropi *et al*. (14) used a combined QM/MM simulation to calculate the absorption and emission peaks of the wtGFP chromophore. Sinicropi *et al*. (14) used the CHARMM (Chemistry at HARvard Molecular Mechanics) molecular dynamics package to calculate molecular motion, and an *ab initio* CASSCF/CASPT2 (Complete Active Space Self-Consistent Field/Complete Active Space with Second-order Perturbation Theory) molecular wavefunction calculation. These calculations (14)] achieved notable accuracy in estimating the positions of the GFP chromophore absorption and emission peaks under a variety of chromophore cavity conditions.

The high-pressure structures of Citrine and associated spectral information should provide a useful test of these more advanced quantum chemical models of fluorescence.

S2. Effects of Pressure on the pH of Citrine Solutions

The fluorescence spectra of members of the *Aequorea* Yellow Fluorescent Protein family, of which Citrine is a member, are known to be sensitive to changes in solution pH (18). This pH sensitivity of the YFPs complicates the analysis of the effects of high pressure on the fluorescence spectrum of Citrine as the pH of many buffers are known to be sensitive to high pressure as high pressure often favors the association or dissociation of protons (19, 20). It was very important to clarify the issue of the independence of Citrine's red shift from solvent conditions, so that it would be appropriate to interpret the fluorescence peak shift in terms of structural changes of the protein, a quantity that is measurable by X-ray crystallography, rather than in terms of changes to the electrostatic environment of Citrine due to changes of pH of the solvent.

Buffers for crystallization and spectroscopy of Citrine were selected for insensitivity to pressure. The buffering properties of Tris and acetate are known to be largely insensitive to pressure (19-21). We are unaware of reports on the pressure sensitivity of HEPES. Additionally, Citrine is known to be less sensitive to changes in pH than other *Aequorea* Yellow Fluorescent Proteins (22).

Citrine displayed an almost identical shift in fluorescence peak in HEPES at pH 7.5, Tris at pH 7.5 and acetate at pH 5.0. This result implies that the fluorescence peak shift of Citrine under pressure observed in our earlier work on Citrine (12) is mechanical in nature, and a direct result of the deformation by pressure of the protein's structure, rather than an effect that is mediated by the protein's solvent. Plots of Citrine's fluorescence peak versus applied hydrostatic pressure at room temperature in different buffering solutions are shown in fig. S4.

S3. Validation of Clustering Algorithm

To further quantify the non-isotropic compression of the Citrine structure under high pressure, we sought to identify groups of atoms in the Citrine structure that move in concert under the application of high pressure. The high pressure structures of hen egg white lysozyme (6, 10) and of T4 lysozyme (9) show the existence of domains of differing compressibility.

The existence of groups of residues that move in concert with increasing pressure was first suggested by manual inspection of animated distance difference matrices (for an example of a distance difference matrix see fig. S8) of the high-pressure Citrine structures. Each frame in the animation corresponded to a colored, averaged distance difference matrix between the ambient structures of Citrine and the structures at an elevated pressure.

This visual analysis hinted at the presence of residues that maintained an approximately constant distance between one another with increasing pressure, yet showed varying distances between themselves and other residues not in the cluster. However, this visual analysis was tedious, and somewhat sensitive to the vagaries of the eye and mind of the inspector. The eye of the author is much more sensitive to the motion present in these animations, and is poor at selecting these patterns in a static image. For this reason, while it was easy to gain a sense that some sort of concerted motion was occurring in the Citrine molecule with elevated pressure, it was hard for

the author to definitively draw boundaries between these clusters. Thus, an automated procedure was desired, that would analyze these distance difference maps, and examine them for internal correlations. The proprietary clustering algorithm RIGIMOL that is incorporated into the molecular graphics and manipulation program PyMOL (DeLano Scientific LLC, Palo Alto, CA, USA) performs this task: automated analysis of distance difference matrices between structures. RIGIMOL was originally developed to interpolate between two or more distinct structures of a protein, for instance between the open and closed states of a hinged protein, and produce a trajectory between the two states, for the purposes of producing an animation of the trajectory.

RIGIMOL rapidly identified what we believe to be the defining feature of the Citrine deformation: the presence of two groups of residues that compose the β-barrel. As protein domains tend to be visually distinguishable, while the Citrine molecule is at first inspection, cylindrically symmetrical, these groups of residues were termed *clusters*. It was very important to definitively validate the cluster assignment produced by the RIGIMOL algorithm, to reduce the possibility that the identification of these two clusters was simply an artifact of the clustering algorithm, perhaps due to random coordinate error due to coordinate uncertainty in the Citrine structure. For this reason, the clustering algorithm was re-run many times with different Citrine structures, different portions of the Citrine structure, different refinement model-sets and different values for the clustering algorithm parameters. The reproducibility of the clustering assignment was checked in each of these cases.

While these clustering-assignment reproducibility experiments consistently identified the presence of two clusters in the β-barrel of the Citrine molecule, the location, relative size, and boundary between these two clusters varied from experiment to experiment.

The RIGIMOL algorithm permits the user to select a variety of clustering parameters including the maximum allowed aspect ratio of a cluster and threshold positional and angular displacements above which atoms are no longer considered part of a cluster and the minimum size of a cluster. It was found that the cluster-assignment, at least in the case of Citrine, was largely insensitive to the clustering algorithm parameters.

The cluster-assignment reproducibility experiments found that the clustering assignment is heavily dependent upon the choice of input structures. RIGIMOL takes a series of structures as an input. However, RIGIMOL cannot interpret sequences of structures containing multiple equivalent structures, for instance, two structures at the same pressure. For this reason, multiple sequences with different structures at each pressure were tried. The experiments were also repeated with sequences of structures derived from two different sets of high-pressure atomic models of Citrine. Refinement set 1 was derived from diffraction data that was truncated at a resolution where the average signal-to-noise calculated by SCALA ($\langle I \rangle / \langle \sigma \rangle$) was 3.0. Refinement set 2 was derived from same original diffraction data, but was not truncated. The models included in refinement set 2 are listed in table S1 and were deposited in the Protein Data Bank. The analysis presented in this article uses the Citrine atomic models from refinement set 2.

The sensitivity in the results of the clustering assignment to the choice of input structures is intuitively understandable. Some regions of the Citrine structure: the N-terminal α-helix, the C-terminus and the floppy β-strand composed of residues 143 to 148 show disorder and are highly variable from structure to structure, even at the same pressure. For this reason, it was suspected that random errors in the positions of atoms in these regions would bias the clustering analysis,

and mask the real, but smaller pressure-induced concerted motions present in the well-ordered β-barrel scaffold. For this reason, we focused on finding a subset of the Citrine structure that would produce highly similar clustering results independent of the choice of input structures.

We found that the subset of the Citrine molecule that produced the most reproducible clustering assignment consisted of the central 3-10 helix and β-barrel walls, without the floppy β-strand composed of residues 143 to 148. Fig. S5 shows the results of the clustering analysis for refinement sets 1 and 2. The results of the clustering assignment, using the reduced Citrine structure shown in fig. S5, appear to be highly similar, independent of refinement set. This gives some confidence that the deformation motion identified by the RIGIMOL algorithm is real, and not an artifact of the algorithm.

S4. Volume Reduction of Citrine Molecule Under Pressure

The overall volume of the Citrine molecule reduces under high pressure. The external surface and surfaces of internal cavities present in each solvent-stripped Citrine structure were identified and traced with the reduced surface computation program MSMS (23) using a 1.2 Å radius probe. The surfaces identified by MSMS were used to compute the volume enclosed by the external surface of each Citrine structure (the *excluded volume*) and the volumes of the cavities present in the interior of each Citrine structure. The *net volume* of each structure was computed by subtracting the total internal cavity volume from the excluded volume of the structure. Plots of the averaged excluded volume and averaged net volume of the solvent-stripped Citrine structures are shown as a function of pressure in fig. S7.

Both the excluded volume and net volume of Citrine decrease by approximately 300 $Å^3$, or 1.1% over the 500 MPa pressure range investigated. The equal reduction of the excluded and net volumes of Citrine indicates that the volume reduction of the molecule is not accounted for solely by reduction in internal cavity volume. The volume reduction of Citrine over the 500 MPa pressure range gives an isothermal compressibility of

$$\beta = \left(-\Delta V/\Delta P\right)/V_{\text{Initial}} = 2.35\ \text{MBar}^{-1} = 2.35 \times 10^{-2}\ \text{GPa}^{-1} \qquad \text{(S4.1)}$$

This value is at the low end of the protein compressibility range reported by Heremans and Smeller (24). The inverse of the isothermal compressibility, the isotropic bulk modulus of Citrine is $K = 42.5$ GPa. For comparison: $K_{\text{Steel}} \approx 160$ GPa and $K_{\text{Aluminum}} \approx 76$ GPa.

S5. Calculation of Noise Threshold on Structural Deformation

A plot of the average displacement of the α-carbon of each residue under a pressure increase from ambient pressure to 400 MPa was shown in fig. 2 of the main text. Fig. 2 shows an estimated noise threshold of ≈ 0.2 Å, below which we believe pressure-induced deformations to the Citrine structure cannot be definitively identified.

By adding the estimated standard uncertainties on the structures of Citrine shown in table S1 in quadrature, we can estimate that the uncertainty in the displacements between pressures: the "noise threshold" seen in fig. 2 (9, 11). Explicitly, we believe that the estimated standard uncertainty on a displacement of an atom, Δx, between two pressure levels, P_0 and P_1, should be estimated by the estimated standard coordinate uncertainties at the two pressure levels, $\sigma\left(x,P_0\right)$ and $\sigma\left(x,P_1\right)$;

$$\Sigma\left(\Delta x,P_0,P_1\right)=\sqrt{3}\left(\sigma\left(x,P_0\right)^2+\sigma\left(x,P_1\right)^2\right)^{1/2} \tag{S5.1}$$

The $\sqrt{3}$ term is incorporated to account for the possibility that the error the coordinates of the atom at each pressure may not be in the same dimension. The Cruickshank uncertainty formula (15) estimates the uncertainty on each component of coordinate of an atom, rather than in the position. To account for the uncertainty in a position, the coordinate uncertainty must be multiplied by $\sqrt{3}$ (15). Thus, for fig. 2

$$\begin{aligned}\Sigma\left(\Delta x,0.1\text{ MPa},400\text{ MPa}\right)&=\sqrt{3}\left(0.114^2+0.111^2\right)^{1/2}\\&=1.59\sqrt{3}\text{ Å}\\&=0.27\text{ Å}\end{aligned}\quad . \tag{S5.2}$$

It is worth noting, that the apparent noise threshold in fig. 2 is ≈ 0.2 Å, suggesting that the error estimate of 0.27 Å may be slightly too large. This is certainly possible as the Cruickshank error estimation formula only accounts for the diffraction data contribution to the error on the structure (15). Geometric constraints applied in the refinement of these structures may assist in noticeably reducing the noise threshold for detection of pressure induced perturbations, at least at the maximum diffraction resolutions, 1.5 to 2.5 Å, observed in these experiments (15).

S6. Changes to Secondary and Tertiary Structure of Citrine Under High Pressure

Although the displacement plot shown in fig. 2 of the main text shows the magnitude of structural changes due to pressurization, it does not provide information on the directions of these motions. To further understand the deformation of the Citrine molecule under pressure, a distance difference matrix (10) was calcuated, showing the expansion and contraction of distances between residue pairs in the Citrine structure under a pressure increase from 0.1 to 400 MPa. The distance difference matrix shown in fig. S8 indicates that Citrine does not uniformly compress with pressure: some distances compress (blue regions in fig. S8), while others expand (red regions in fig. S8) with increasing pressure. The white regions in fig. S8 indicate distances that either compress by more than 0.6 Å, or expand by more than 0.4 Å. The largest expansion of a distance in the whole molecule is by ≈ 2.7 Å, while the largest compression of a distance is by ≈ 1.7 Å. At least one of the residues in the atom pairs that show these large distance compressions and expansions are often observed at the N-terminus of the Citrine molecule. The

largest distance compression between residues in the β-barrel is 0.92 Å, and the largest expansion is 0.67 Å.

There are numerous residues that are displaced by several times the noise threshold on the pressure-induced displacement of residues in the Citrine structure. The largest of the deviations in fig. 2 of the main text are at the start (N-terminus) of the primary sequence. This may in part be due to a change in secondary structure of this region with increasing pressure. Calculation of the secondary structure of Citrine with DSSP (25) indicates that the first 10 residues (Pro-1 to Phe8) form an α-helix at ambient pressure. However, with increasing pressure, the number of residues in the N-terminal α-helix is reduced. In structures above 125 MPa, Phe8 consistently (14 out of 16 structures) is no longer part of the α-helix. Leu7 also is not part of the helix in 10 of 16 structures above 125 MPa. The N-terminal residues Pro-1 and Met0 are not part of the helix in 5 of 7 structures above 200 MPa.

However, the large displacements at the N-terminus seen in fig. 2 of the main text cannot be attributed solely to pressure. The N-terminus α-helix and loops of Citrine have poorly resolved electron density, indicating disorder. The variation in α-carbon position between any two structures at the same pressure in the series of high-pressure Citrine structures is of similarly large magnitude to that seen in fig. 2. It is interesting to note that N-terminal primary sequence deletions up to Phe8, the same residues that show changes of secondary structure with increasing pressure, have no impact on the folding or maturation of the Green Fluorescent Protein (26). This suggests that changes of the secondary structure up to Phe8, while notable, do not affect the spectral properties of Citrine. Additionally, the N or C terminus (or both) of YFP and other *Aequorea* fluorescent proteins can be fused to other materials, including proteins, without changing the spectral properties of the molecule (27). Therefore, we believe that these large spatial deviations seen at the N-terminus are decoupled from the pressure-induced actuation of the chromophore deformation.

The secondary structure of the 3-10 helix that fills the center of the β-barrel and the walls of the β-barrel is retained up to at least 500 MPa. These results are consistent with the spectroscopic observations by Scheyhing *et al*. (28) and Herberhold *et al*. (29) that suggest that the tertiary structures of *Aequorea* fluorescent protein molecules are stable to unfolding until pressures of at least 900 MPa and up to 1300 MPa for many mutants.

In addition to the displacements seen at the disordered N-terminus region of Citrine, there are numerous residues that also displaced by several times the noise threshold. Two notable displacements highlighted in fig. 2 are the pressure-induced displacements of residues 66 (the main chromophore) and Tyr203, consistent with our previous report of the deformation of the chromophore (12). It is noted that the magnitudes of the residue displacements are non-uniform, suggesting non-isotropic compression of Citrine.

S7. Inertia Tensor Analysis of Citrine β-barrel Scaffold

The principal axes of the Citrine β-barrel wall were computed (30) to provide more intuitive insight into the pressure-induced deformation of Citrine. The residues involved in β-sheet

interactions in the β-barrel region of the Citrine molecule were extracted from the series of high-pressure Citrine structures. The analysis was limited to the β-barrel wall to avoid being dominated by the disordered regions of the structure. The α-carbons of the extracted structures were first aligned using the least squares fitting algorithm incorporated into PyMOL (DeLano Scientific LLC, Palo Alto, CA, USA) prior to computing the inertia tensor of each structure. The principal axes of each β-barrel structure were found by computing the eigenvectors of the structure's inertia tensor and associated eigenvalues using the NumPy numerical library. A diagram showing the orientation of the principal axes of the Citrine β-barrel at ambient pressure is shown in fig. S10A. The number 2 principal axis is directed approximately along the cylindrical symmetry axis. Principal axes 1 and 3 are mutually perpendicular and lie approximately in the plane of cylindrical symmetry.

As the Citrine molecule is pressurized, the number 1 β-barrel wall principal axis remains largely fixed in direction relative to the reference frame defined by the alignment of the β-barrel structures. The other two principal axes, 2 and 3, approximately rotate about principal axis 1. A plot of the averaged angular deviation of principal axis 3 from its room pressure direction is shown in fig. S10B. The angular deviation of principal axis 3 from its room pressure direction proceeds linearly up to the maximum pressure observed of 500 MPa at a rate of ≈ 0.5˚ per 100 MPa. The directions of drift of principal axes 2 and 3 are shown in fig. S10A. The slight re-orientation of the principal axes of the Citrine β-barrel wall indicates a redistribution of mass on the wall of the Citrine β-barrel. The direction of the drift of the principal axes suggests a motion of mass towards the side of Citrine β-barrel to which the perturbing Tyr203 ring is attached (see fig. S10A).

The eigenvalues of the inertia tensor of the Citrine β-barrel wall are an indicator of the radius of the β-barrel wall and the height of the β-barrel. For an ideal, thin walled cylinder of mass m, radius r and height h, the eigenvalue associated with the principal axis aligned with the cylindrical symmetry axis is

$$I_z = \frac{mr^2}{2} \tag{S7.1}$$

The eigenvalues associated with the principal axes lying in the cross section of the thin walled cylinder are

$$I_x = I_y = \frac{m}{12}\left(3r^2 + h^2\right) \tag{S7.2}$$

Given that the amino acid mass of the cylinder is constant, the eigenvalues are sensitive indicators of the dimensions of the cylinder.

While the eigenvalues associated with principal axes 1 and 3 reduce with pressure, the eigenvalue associated with principal axis 2 remains relatively constant. The reduction of eigenvalues 1 and 3 is consistent with the overall compression of the molecule under pressure of approximately 1.1% over 500 MPa. However, the constancy of eigenvalue 2 suggests that the side of the β-barrel wall close to principal axis 2 may not be compressing. This observation

indicates that rather than isotropically compressing, part of the wall of the β-barrel in the vicinity of principal axis 2 may be retaining its original radius of curvature, appearing to bulge out as other sections of the wall reduce in radius of curvature. The Citrine molecule β-barrel appears to be bending under pressure, in a manner reminiscent of the bending of a bimetallic strip under heating.

S8. Perturbation of Hydrogen Bonding Network in Chromophore Cavity

Most of the hydrogen bonds in the chromophore cavity hydrogen bonding network show very small changes in length with increasing pressure. The distance between the Leu68 amide nitrogen and the solvent molecule HOH-2 (bond 3 in fig. S10A) shows no variation with pressure. The chromophore oxygen-2 to Arg96 amide nitrogen distance (bond 2 in fig. S10A) varies by less than 0.1 Å over 500 MPa, as does the Tyr203 phenolic oxygen to HOH-2 distance (bond 4 in fig. S10A). The Ser205 γ-oxygen to the HOH-1 solvent molecule distance (bond 7 in fig. S10A) compresses by 0.1 Å over the pressure range 0.1 to 50 MPa, and then remains constant up to a pressure of 500 MPa. The bond between the chromophore phenolic oxygen and HOH-1 (bond 8 in fig. S10A) increases in length by ≈ 0.1 Å at a pressure ≈ 250 MPa, and then recompresses to its original length by 500 MPa. The bond between the carbonyl oxygen of Asn146 and HOH-1 (bond 9 in fig. S10A) also expands by ≈ 0.25 Å at a pressure of 250 MPa, and the recompresses by 0.2 Å by 500 MPa.

Three bonds that do show large variations with pressure are those between the His148 δ_1-nitrogen and the chromophore phenolic oxygen (bond 1 in fig. S10A), the Glu222 ε_1-oxygen and the HOH-2 solvent molecule (bond 5 in fig. S10A), and chromophore nitrogen-2 and Glu222 ε_2-oxygen (bond 6 in fig. S10A). The bond 1 (fig. S10A) distance increases by 0.4 Å over 500 MPa, while bond 5 and bond 6 (fig. S10A) compress from 3.8 to 3.4 Å and 4.0 to 3.0 Å over 500 MPa, respectively.

S9. Speculation on Modifications to Citrine Structure

We speculate that the structural information available on Citrine at high pressure may inspire structural modifications to Citrine that may permit the Citrine molecule to remain in the blue-shifted transient state observed by Blum *et al.* (31) for longer, or even permanently stabilize it. It may be possible to induce the bending of the Citrine scaffold seen at high-pressure under ambient conditions by repacking the Citrine scaffold by mutating or adding residues along the interface of these two clusters. On this basis, fig. S12 shows several possible sites where one would logically seek to introduce mutations. To replicate the bending seen at high pressure, it is required that cluster 1 move down and to the right in fig. S12. It is interesting to consider if this may be achieved by simultaneously mutating residues on the left hand interface between clusters 1 and 2 to bulkier residues, and mutating those on the right hand interface to less bulky residues, while keeping other properties of the residues as similar as possible. On the left hand side, possible mutations may be Phe46 to Tyr or Trp, Val16 to Leu, Ile or Met, Asn121 to Gln, Val112 to Leu, Ile or Met, Tyr92 to Trp. On the right hand side, these mutations may be Ile161

to Val, Ala or Gly; Gln183 to Asp, Cys, Thr or Ser; Val163 to Ala or Gly; while leaving Phe165 unchanged, as it is the smallest aromatic amino acid. The success of this strategy would depend upon the perturbations of these mutations being small enough to not affect the folding of the β-barrel scaffold. While a green-shifted YFP is of little practical value, it would be an important proof of principle. If structural perturbations due to pressure of this nature are observed in catalytic proteins, it may be possible to use a structural perturbation approach similar to the one suggested for Citrine to suggest mutations to bias a population of catalytic molecules into move active conformations, resulting in an acceleration in the bulk rate of catalysis.

Recent single molecule experiments on enzymes including cholesterol oxidase (32), hairpin ribozyme (33), λ exonuclease, lipase (34, 35) and the Yellow Fluorescent Protein (31) indicate that under ambient conditions, single protein molecules switch between a series of conformational states with distinct functional properties (36). Some of these transiently occupied states have higher activities than a bulk sample of the enzyme (the time-averaged activity of a single enzyme). If it were possible to somehow stabilize the transiently occupied states, or just enhance the lifetime of these states, then the bulk rate of the enzyme could be enhanced.

Experiments by Urayama *et al*. (11, 37) indicate that the high-pressure structure of sperm whale myoglobin corresponds to a transiently occupied room temperature, room pressure substate of sperm whale myoglobin. We believe that the high-pressure structures of Citrine that we have presented in this report, also corresponds to a transiently occupied state of Citrine at room temperature and pressure: the green-emitting state seen by Blum *et al.* (38).

High pressure is known to alter the activity of many proteins (39). Using high-pressure stopped flow techniques Ueda *et al*. (40) observed that pressures in the range of tens of MPa reduce the flash decay rate of firefly luciferase. Bruner and Hall (41) used a high-pressure patch clamp apparatus to measure the conductance properties of the pore forming membrane protein alamethicin. Bruner and Hall found that pressures up to 100 MPa exponentially increase the average lifetime of the conductance states of alamethicin. Carey *et al.* (42) noted that the oxygen binding affinity of human hemoglobin samples is increased by the application of pressures in the range of 100 MPa. Carey *et al.* found that the R (relaxed or oxygenated) to T (tense or de-oxygenated) transition of hemoglobin is unaffected by the application of pressure, suggesting that the oxygen binding affinity of the individual hemoglobin subunits is enhanced by the application of pressure. Adachi and Morishima (43) established that the rate of carbon monoxide and oxygen association of horse and sperm whale myoglobin are exponentially modified by pressures up to 200 MPa using time resolved spectroscopy and flash photolysis. Miller *et al.* (44) observed that the methyl-viologen reducing activity (a proxy for H_2 consumption) of a hydrogenase from the thermophilic bacterium *Methanococcus jannaschii* is increased by the application of pressures up to 75 MPa. Hay *et al*. (45) observed that pressures up to 200 MPa exponentially increase the rate of NADH oxidation by the flavoprotein morphinone reductase.

It is possible that in some of these cases, the altered activity of these proteins is due to the molecule increasing the time it spends in conformations that are only transiently occupied at ambient pressure, or continuously transforming into a conformation that closely resembles a transient state at ambient pressure.

If it could be shown that a high-pressure atomic structure of one of these enzymes corresponding to a structural state with an enhanced rate constant, then it might be possible to use the approach first attempted with Citrine to stabilize the structure of the enzyme with the enhanced rate constant, and increase the bulk rate constant of the enzyme.

Supporting Tables

Protein Data Bank Accession Code	*Pressure (MPa)*	*ESU Free R (Å)*
3DPW	0.1	0.17
3DQO	0.1	0.12
3DQN	50	0.11
3DQM	75	0.11
3DQL	100	0.12
3DQK	100	0.12
3DQJ	100	0.14
3DQI	100	0.12
3DQH	100	0.11
3DQF	100	0.11
3DQE	125	0.11
3DQD	125	0.14
3DQC	125	0.13
3DQA	125	0.1
3DQ9	150	0.11
3DQ8	150	0.14
3DQ7	192	0.07
3DQ6	192	0.14
3DQ5	196	0.12
3DQU	200	0.11
3DQ4	200	0.11
3DQ3	250	0.15
3DQ2	400	0.13
3DQ1	400	0.16
3DPZ	400	0.15
3DPX	500	0.11

Table S1: Protein Data Bank accession codes for Citrine structures used in the analysis presented in this article. The ESU (Estimated Standard Uncertainty) shown in column 3 was estimated by Cruickshank's R_{Free} based positional uncertainty formula (15).

References

1. Mealli, C., and D. M. Proserpio. 1990. MO Theory Made Visible. Journal of Chemical Education 67:399-402.

2. Cramer, C. J. 2004. Essentials of computational chemistry : theories and models. Wiley, Chichester, West Sussex, England ; Hoboken, NJ.

3. Hoffmann, R. 1963. An Extended Hückel Theory .I. Hydrocarbons. In J Chem Phys. 1397-&.

4. Heikal, A. A., S. T. Hess, G. S. Baird, R. Y. Tsien, and W. W. Webb. 2000. Molecular spectroscopy and dynamics of intrinsically fluorescent proteins: coral red (dsRed) and yellow (Citrine). Proc. Natl. Acad. Sci. U.S.A. 97:11996-12001.

5. Lakowicz, J. R. 2006. Principles of fluorescence spectroscopy. Springer, New York.

6. Refaee, M., T. Tezuka, K. Akasaka, and M. P. Williamson. 2003. Pressure-dependent changes in the solution structure of hen egg-white lysozyme. J Mol Biol 327:857-865.

7. Williamson, M. P., K. Akasaka, and M. Refaee. 2003. The solution structure of bovine pancreatic trypsin inhibitor at high pressure. Protein Sci 12:1971-1979.

8. Collins, M. D., G. Hummer, M. L. Quillin, B. W. Matthews, and S. M. Gruner. 2005. Cooperative water filling of a nonpolar protein cavity observed by high-pressure crystallography and simulation. Proc Natl Acad Sci USA 102:16668-16671.

9. Collins, M. D., M. L. Quillin, G. Hummer, B. W. Matthews, and S. M. Gruner. 2007. Structural rigidity of a large cavity-containing protein revealed by high-pressure crystallography. J Mol Biol 367:752-763.

10. Kundrot, C., and F. Richards. 1987. Crystal structure of hen egg-white lysozyme at a hydrostatic pressure of 1000 atmospheres. J Mol Biol 193:157-170.

11. Urayama, P. K., G. N. Phillips, and S. M. Gruner. 2002. Probing substates in sperm whale myoglobin using high-pressure crystallography. Structure 10:51-60.

12. Barstow, B., N. Ando, C. U. Kim, and S. M. Gruner. 2008. Alteration of citrine structure by hydrostatic pressure explains the accompanying spectral shift. Proc Natl Acad Sci U S A 105:13362-13366.

13. Isaacs, N. S., K. Javaid, and E. Rannala. 1978. Reactions At High-Pressure .5. Effect Of Pressure On Some Primary Kinetic Isotope Effects. J. Chem. Soc.-Perkin Trans. 2:709-711.

14. Sinicropi, A., T. Andruniow, N. Ferré, R. Basosi, and M. Olivucci. 2005. Properties of the emitting state of the green fluorescent protein resolved at the CASPT2//CASSCF/CHARMM level. J Am Chem Soc 127:11534-11535.

15. Cruickshank, D. 1999. Remarks about protein structure precision. Acta Crystallogr D Biol Crystallogr 55 (Pt 3):583-601.

16. Toniolo, A., S. Olsen, L. Manohar, and T. Martínez. 2004. Conical intersection dynamics in solution: The chromophore of Green Fluorescent Protein. Faraday Discuss 127:149.

17. Niwa, H., S. Inouye, T. Hirano, T. Matsuno, S. Kojima, M. Kubota, M. Ohashi, and F. I. Tsuji. 1996. Chemical nature of the light emitter of the Aequorea green fluorescent protein. Proc Natl Acad Sci U S A 93:13617-13622.

18. Elsliger, M. A., R. M. Wachter, G. T. Hanson, K. Kallio, and S. J. Remington. 1999. Structural and spectral response of green fluorescent protein variants to changes in pH. Biochem. 38:5296-5301.

19. Neuman, R., W. Kauzmann, and A. Zipp. 1973. Pressure Dependence of Weak Acid Ionization in Aqueous Buffers. Journal of Physical Chemistry 77:2687-2691.

20. Zipp, A., and W. Kauzmann. 1973. Pressure Denaturation of Metmyoglobin. Biochem. 12:4217-4228.

21. Gross, M., and R. Jaenicke. 1994. Proteins under pressure. The influence of high hydrostatic pressure on structure, function and assembly of proteins and protein complexes. Eur J Biochem 221:617-630.

22. Griesbeck, O., G. S. Baird, R. E. Campbell, D. A. Zacharias, and R. Y. Tsien. 2001. Reducing the environmental sensitivity of yellow fluorescent protein. Mechanism and applications. J Biol Chem 276:29188-29194.

23. Sanner, M. F., A. J. Olson, and J. C. Spehner. 1996. Reduced surface: an efficient way to compute molecular surfaces. Biopolymers 38:305-320.

24. Heremans, K., and L. Smeller. 1998. Protein structure and dynamics at high pressure. Biochim Biophys Acta 1386:353-370.

25. Kabsch, W., and C. Sander. 1983. Dictionary of protein secondary structure: pattern recognition of hydrogen-bonded and geometrical features. Biopolymers 22:2577-2637.

26. Li, X., G. Zhang, N. Ngo, X. Zhao, S. R. Kain, and C. C. Huang. 1997. Deletions of the Aequorea victoria green fluorescent protein define the minimal domain required for fluorescence. J Biol Chem 272:28545-28549.

27. Tsien, R. Y. 1998. The green fluorescent protein. Annu Rev Biochem 67:509-544.

28. Scheyhing, C. H., F. Meersman, M. A. Ehrmann, K. Heremans, and R. F. Vogel. 2002. Temperature-pressure stability of green fluorescent protein: a Fourier transform infrared spectroscopy study. Biopolymers 65:244-253.

29. Herberhold, H., S. Marchal, R. Lange, C. H. Scheyhing, R. F. Vogel, and R. Winter. 2003. Characterization of the pressure-induced intermediate and unfolded state of red-shifted green fluorescent protein--a static and kinetic FTIR, UV/VIS and fluorescence spectroscopy study. J Mol Biol 330:1153-1164.

30. Foote, J., and A. Raman. 2000. A relation between the principal axes of inertia and ligand binding. Proc Natl Acad Sci USA 97:978-983.

31. Blum, C., A. J. Meixner, and V. Subramaniam. 2004. Room Temperature Spectrally Resolved Single-Molecule Spectroscopy Reveals New Spectral Forms and Photophysical Versatility of Aequorea Green Fluorescent Protein Variants. Biophysical Journal 87:4172-4179.

32. Lu, H. P., L. Y. Xun, and X. S. Xie. 1998. Single-molecule enzymatic dynamics. Science 282:1877-1882.

33. Zhuang, X. W., H. Kim, M. J. B. Pereira, H. P. Babcock, N. G. Walter, and S. Chu. 2002. Correlating structural dynamics and function in single ribozyme molecules. Science 296:1473-1476.

34. Velonia, K., O. Flomenbom, D. Loos, S. Masuo, M. Cotlet, Y. Engelborghs, J. Hofkens, A. E. Rowan, J. Klafter, R. J. M. Nolte, and F. C. de Schryver. 2005. Single-enzyme kinetics of CALB-catalyzed hydrolysis. Angewandte Chemie-International Edition 44:560-564.

35. Flomenbom, O., K. Velonia, D. Loos, S. Masuo, M. Cotlet, Y. Engelborghs, J. Hofkens, A. E. Rowan, R. J. M. Nolte, M. Van der Auweraer, F. C. de Schryver, and J. Klafter. 2005. Stretched exponential decay and correlations in the catalytic activity of fluctuating single lipase molecules. Proceedings of the National Academy of Sciences of the United States of America 102:2368-2372.

36. English, B., W. Min, A. Van Oijen, K. Lee, G. Luo, H. Sun, B. Cherayil, S. Kou, and X. Xie. 2006. Ever-fluctuating single enzyme molecules: Michaelis-Menten equation revisited. Nat Chem Biol 2:87-94.

37. Urayama, P. K. 2001. Techniques for High Pressure Macromolecular Crystallography and the Effects of Pressure on the Structure of Sperm Whale Myoglobin.

38. Blum, C., A. J. Meixner, and V. Subramaniam. 2004. Room temperature spectrally resolved single-molecule spectroscopy reveals new spectral forms and photophysical versatility of aequorea green fluorescent protein variants. Biophys J 87:4172-4179.

39. Frauenfelder, H., N. A. Alberding, A. Ansari, D. Braunstein, B. R. Cowen, M. K. Hong, I. E. T. Iben, J. B. Johnson, S. Luck, M. C. Marden, J. R. Mourant, P. Ormos, L.

Reinisch, R. Scholl, A. Schulte, E. Shyamsunder, L. B. Sorensen, P. J. Steinbach, A. H. Xie, R. D. Young, and K. T. Yue. 1990. Proteins and pressure. J. Phys. Chem. 94:1024-1037.

40. Ueda, I., H. Minami, H. Matsuki, and T. Inoue. 1999. Does pressure antagonize anesthesia? High-pressure stopped-flow study of firefly luciferase and anatomy of initial flash. Biophys J 76:478-482.

41. Bruner, and Hall. 1983. Pressure effects on alamethicin conductance in bilayer membranes. Biophys J 44:39-47.

42. Carey, F., F. Knowles, and Q. Gibson. 1977. Effect of hydrostatic pressure on ligand binding to hemoglobin. J Biol Chem 252:4102-4107.

43. Adachi, S., and I. Morishima. 1989. The Effects Of Pressure On Oxygen And Carbon-Monoxide Binding-Kinetics For Myoglobin - A High-Pressure Laser Flash-Photolysis Study. Journal of Biological Chemistry 264:18896-18901.

44. Miller, J. F., E. L. Almond, N. N. Shah, J. M. Ludlow, J. A. Zollweg, W. B. Streett, S. H. Zinder, and D. S. Clark. 1988. High-pressure-temperature bioreactor for studying pressure-temperature relationships in bacterial growth and productivity. Biotechnol Bioeng 31:407-413.

45. Hay, S., M. J. Sutcliffe, and N. S. Scrutton. 2007. Promoting motions in enzyme catalysis probed by pressure studies of kinetic isotope effects. Proc Natl Acad Sci USA 104:507-512.

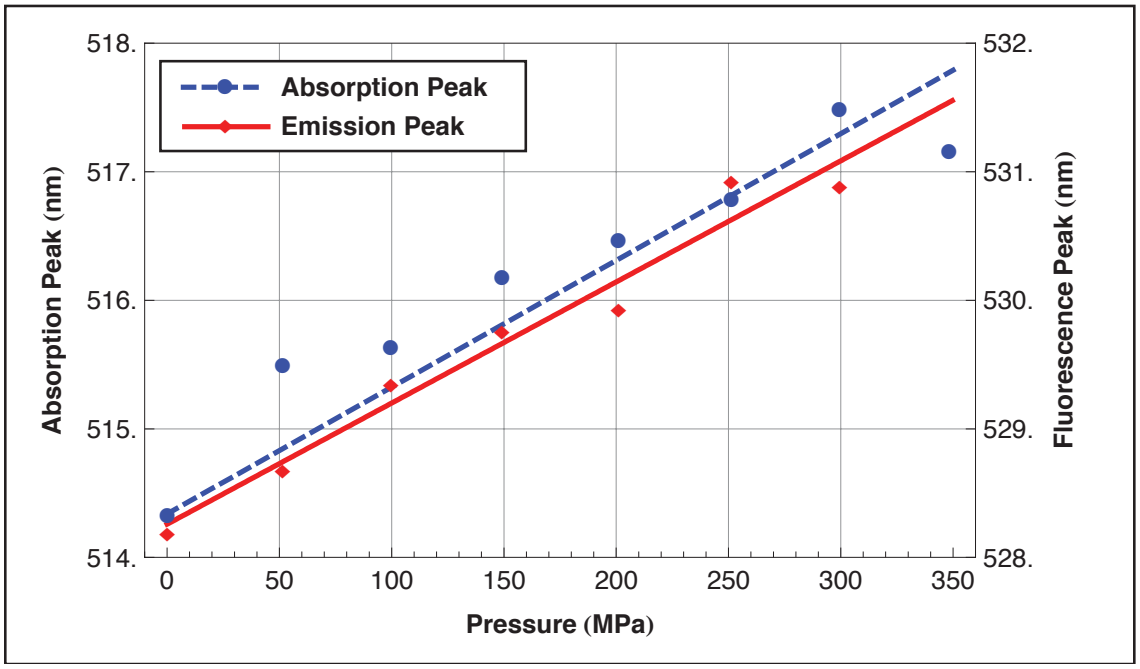

Figure S1: Absorption and emission peaks of Citrine at room temperature in 50 mM HEPES, pH 7.5.

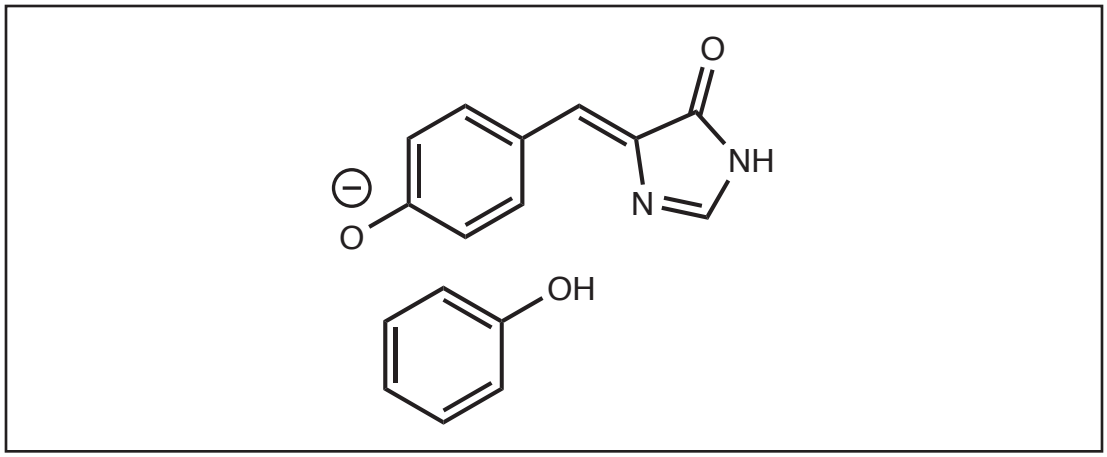

Figure S2: Truncated chromophore structure input to Extended Hückel model of Citrine's fluorescence transition.

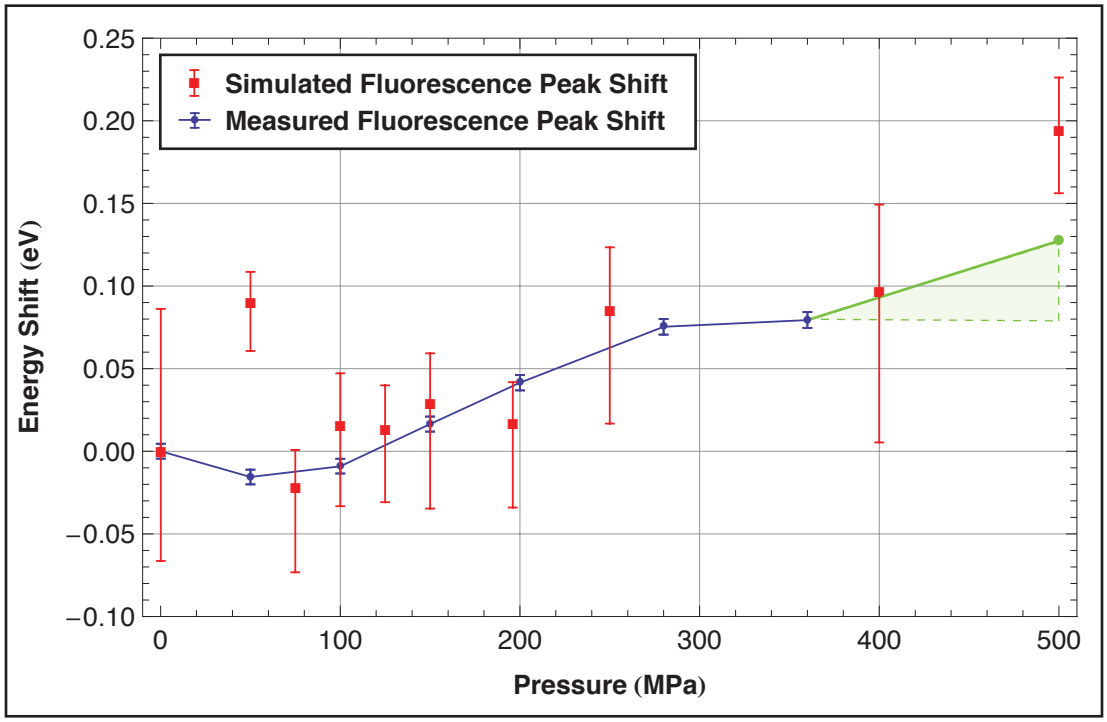

Figure S3: Calculated and observed fluorescence peak energy shift for Citrine under high-pressure cryocooling conditions. The final measured point, at 500 MPa, corresponds to the fluorescence peak energy shift of mEGP relative to Citrine at 0.1 MPa (527 versus 500 nm), and is considered as an estimated upper limit on the fluorescence energy shift of Citrine.

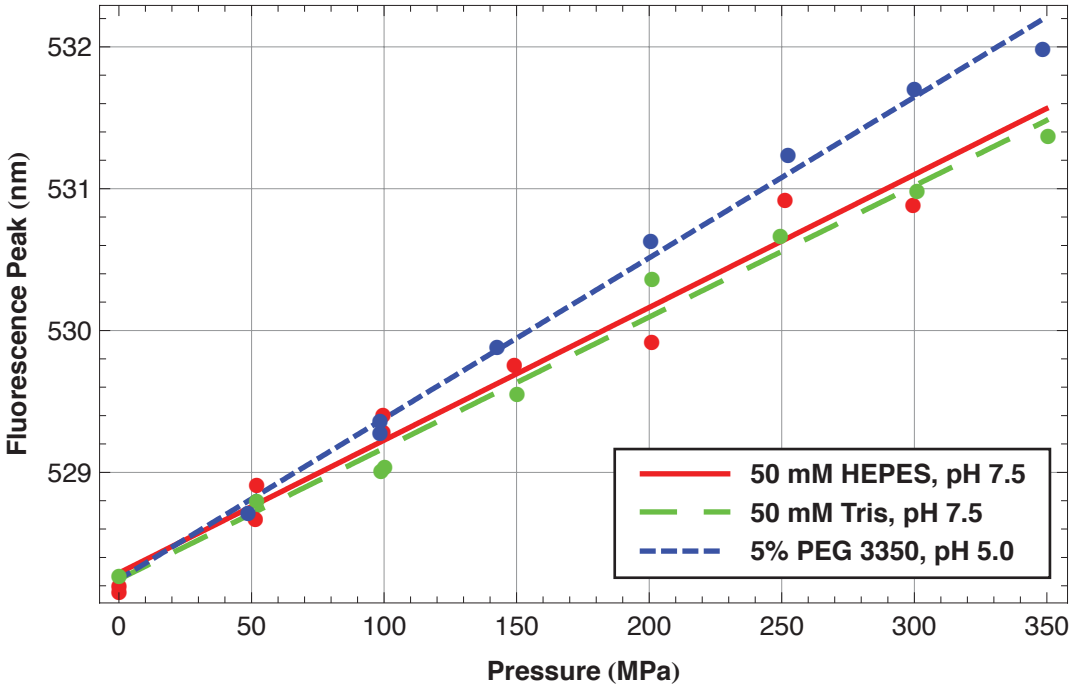

Figure S4: Fluorescence peak shift of Citrine in various buffers at room temperature. Peak shift under pressure was measured using a commercially available high-pressure optical cell (ISS, Urbana-Champaign, IL, USA) and a Chronos spectrophotometer (ISS). The complete solution conditions in the final solution are 5% w/v PEG 3350, 50 mM Na acetate, 50 mM NH_4 acetate, pH 5.0. Adapted from the supporting material of our previously published work on Citrine (12).

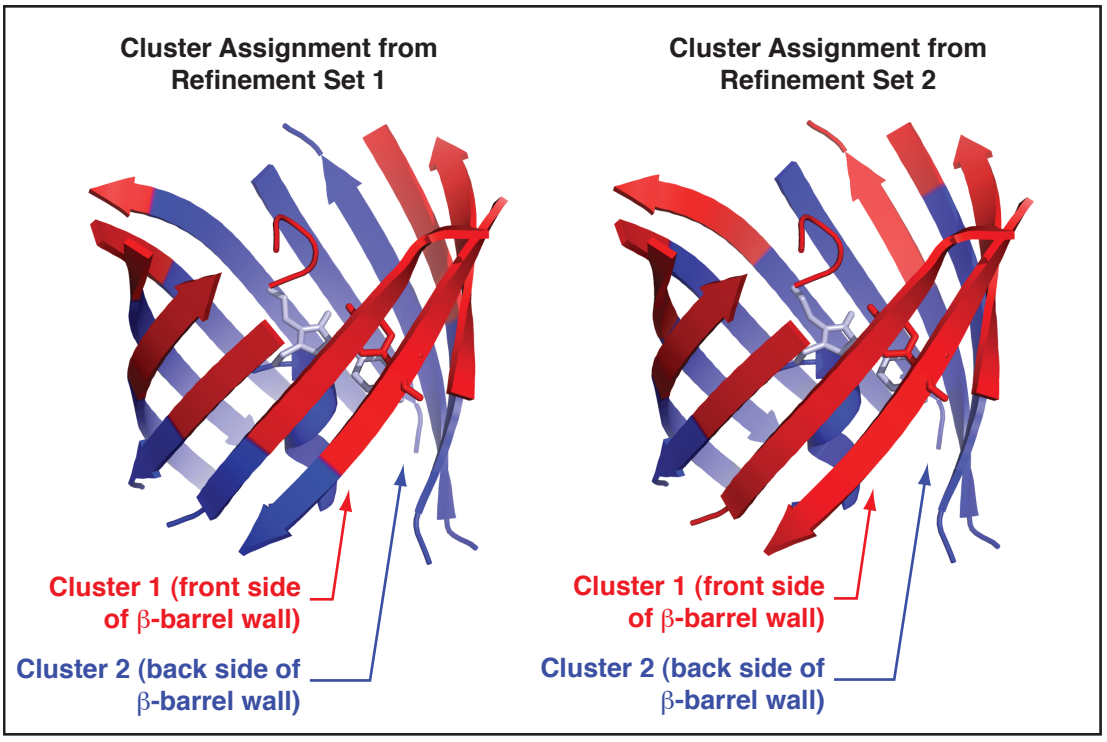

Figure S5: Comparison of the results of RIGIMOL cluster assignment using structures from refinement sets 1 and 2. Cluster 1 is colored red and cluster 2 is colored in blue. The main chromophore, colored in light blue, is attached to cluster 2, while tyrosine 203, colored in red, is attached to cluster 1.

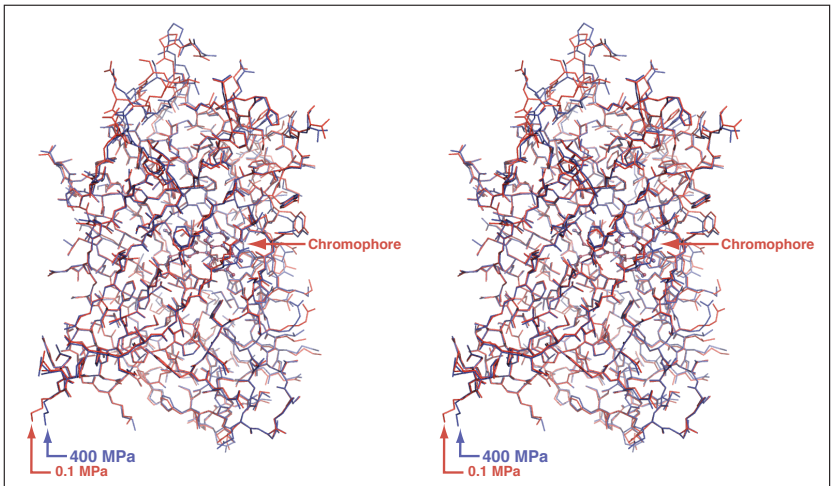

A: Citrine molecule at 0.1 (red) and 400 MPa (blue)

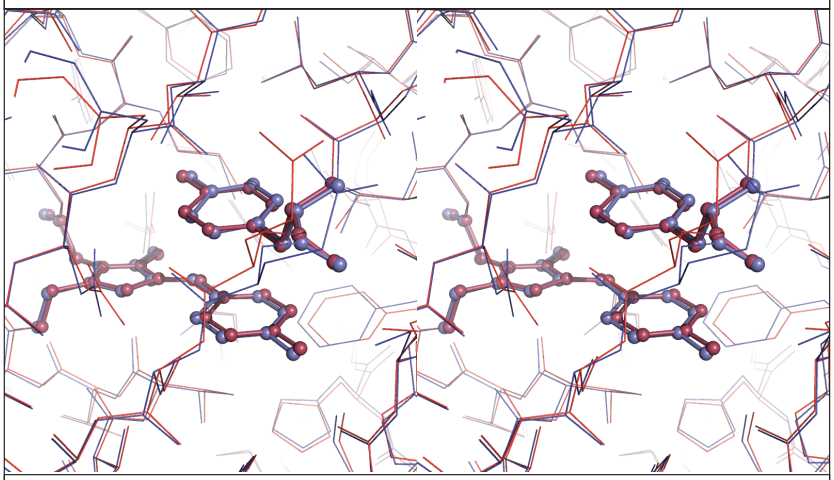

B: Chrompore region of Citrine molecule at 0.1 (red) and 400 MPa (blue)

Fig. S6: Stereo image of superimposed atomic structures of Citrine frozen at 0.1 MPa (red) and 400 MPa (blue).

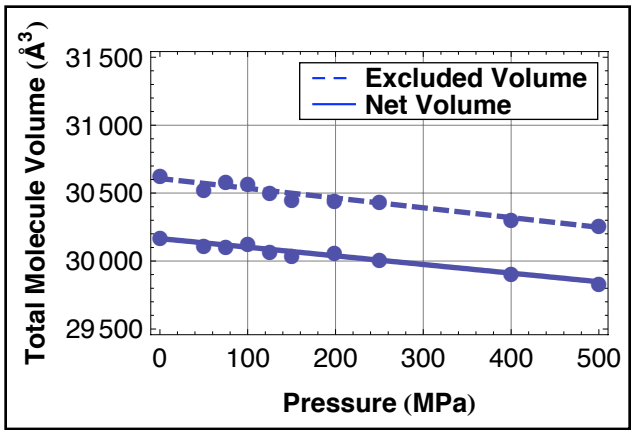

Fig. S7: Averaged excluded volume of the Citrine molecule (dashed line), and averaged net volume of the Citrine molecule (non-dashed line). The net volume is computed by subtracting the internal cavity volume from the excluded volume of the molecule.

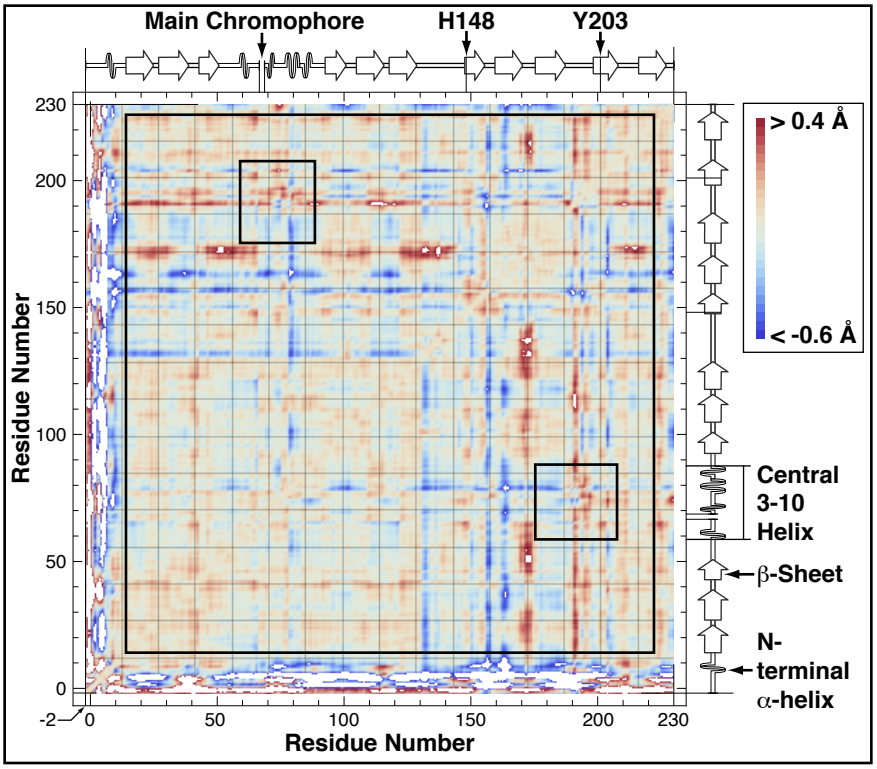

Fig. S8: Averaged distance difference matrix for the Citrine molecule under a pressure increase from 0.1 to 400 MPa. Compressions are shown in blue and expansions are shown in red. The matrix is symmetrical about the diagonal that runs from lower left to upper right of the matrix. Note that all elements on this diagonal are zero. The white regions in the matrix, predominantly at the periphery of the protein structure, indicate distances that either compress by more than 0.6 Å, or expand by more than 0.4 Å. The largest expansion of a distance is by ≈ 2.7 Å, while the largest compression of a distance is by ≈ 1.7 Å. The largest expansion of a distance in the β-barrel and central 3-10 helix region, marked by the large black square is ≈ 0.9 Å, and the largest compression is ≈ 0.7 Å. Note the smaller rectangles marking the expansion of the distance from the central 3-10 helix to the section of the β-barrel containing Tyr203.

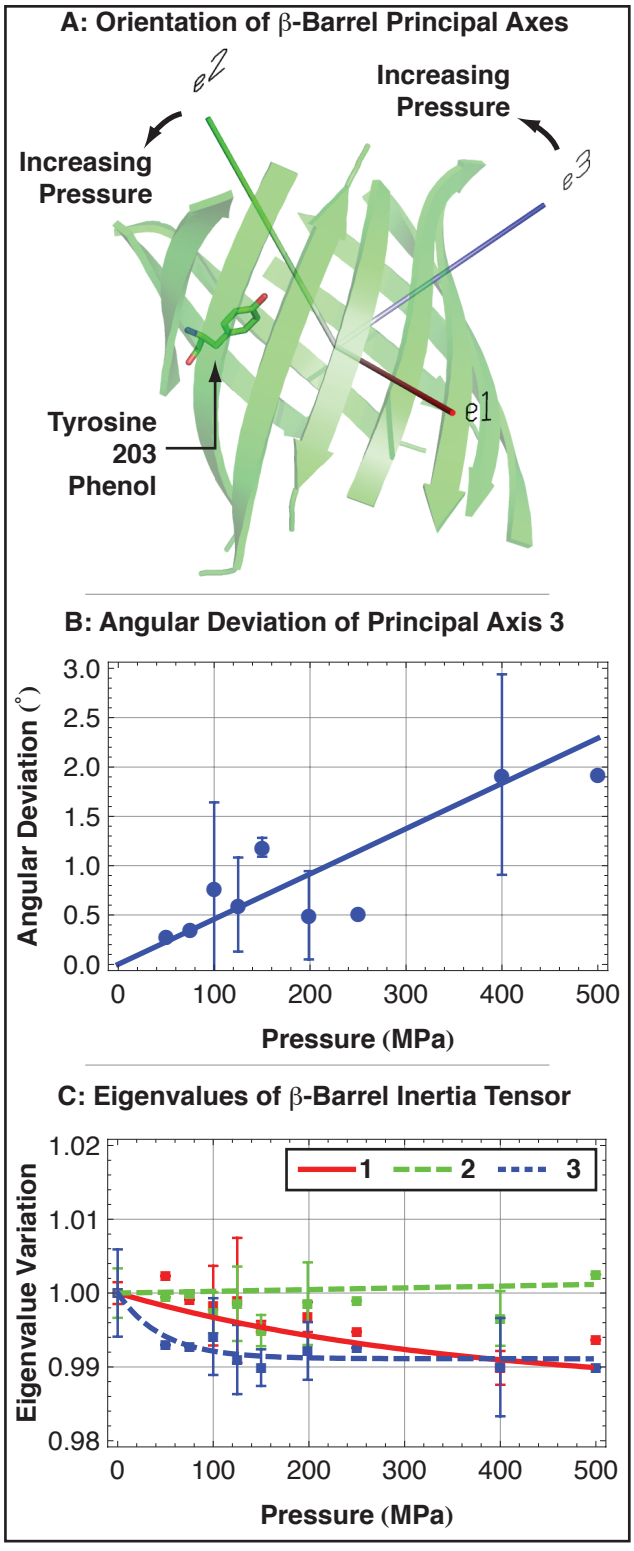

Fig. S9: A: Orientation of the principal axes of the Citrine β-barrel walls at ambient pressure. Arrows indicate the direction of rotation of principal axes 2 and 3 with increasing pressure. B: Angular deviation of principal axis 3 with increasing pressure. C: Variation of the eigenvalues of the inertia tensor of the β-barrel walls with increasing pressure. Eigenvalues 1 (red) and 3 (blue - dotted) reduce by approximately 1% over the pressure range from 0.1 to 500 MPa. Eigenvalue 2 (green - dashed) increases by approximately 0.2% over the same pressure range.

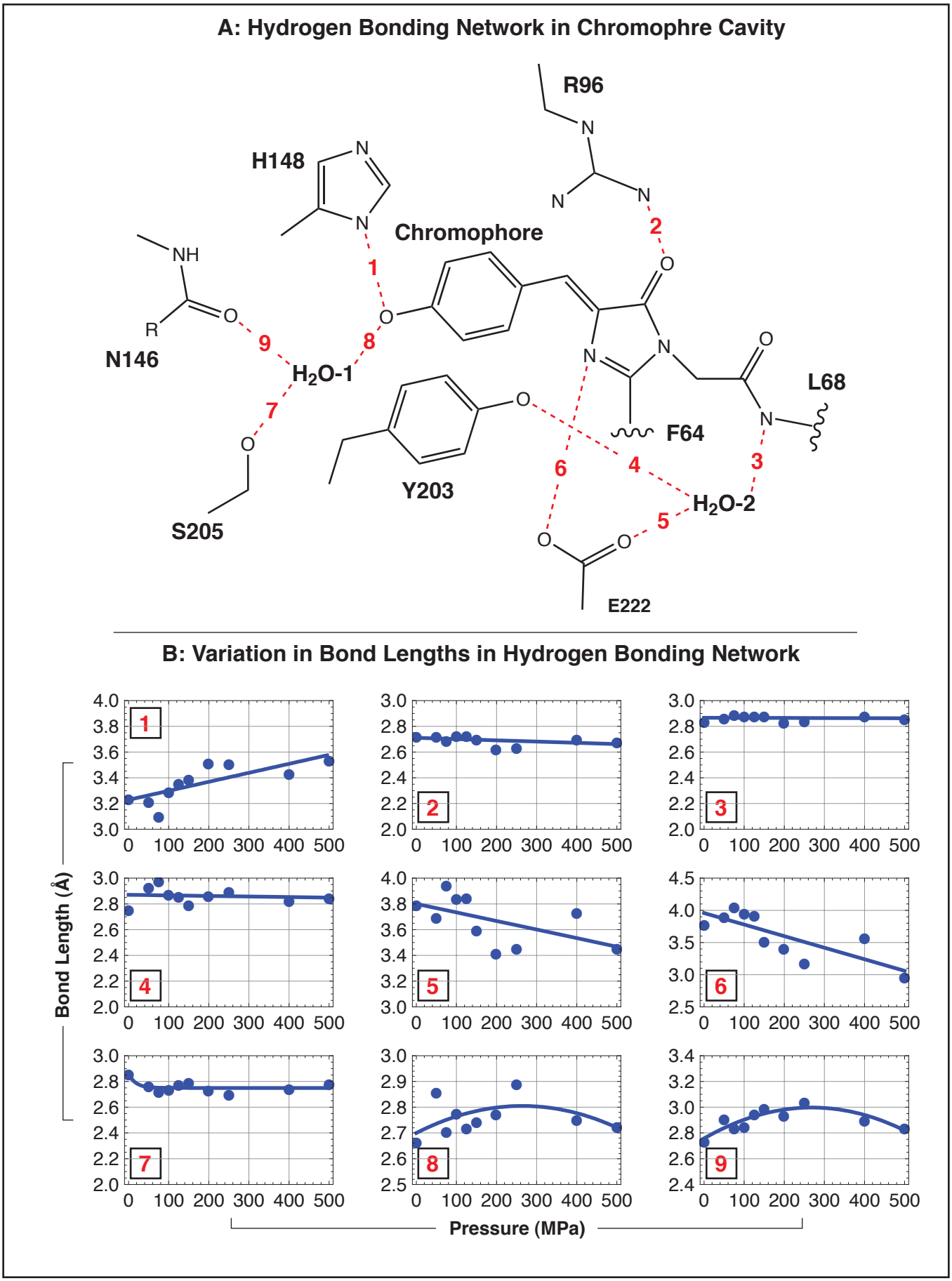

Figure S10: A. Hydrogen-bonding network in Citrine chromophore cavity. B. Variation of lengths in chromophore cavity with pressure.

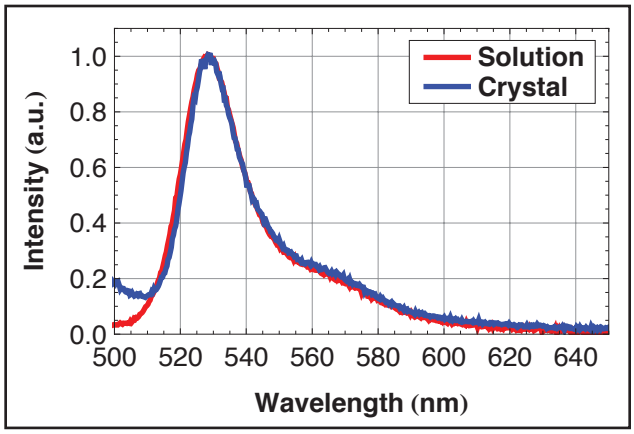

Fig. S11: Comparison of the fluorescence spectra of a flash frozen Citrine solution and a very small, flash frozen Citrine crystal. The Citrine solution is composed of 1 mg/mL Citrine and 5% PEG 3350, 50 mM Na Acetate, 50 mM NH_4 Acetate, pH 5.0, the same buffer conditions as the crystal.

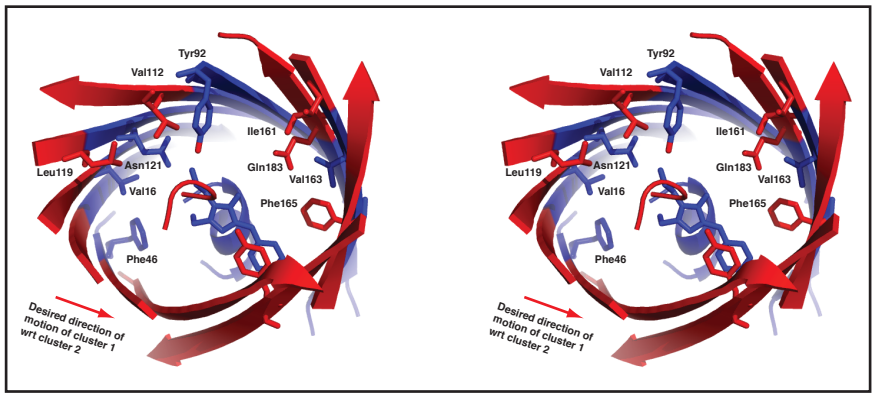

Fig. S12: Stereo pair showing speculated mutation sites that may induce bending of Citrine scaffold under ambient conditions. We speculate that it may be possible to induce the bending of the Citrine scaffold seen in fig. 5 of the main text, and drawn as a cartoon in fig. 8 of the main text, by introducing small to large mutations on the left side of the molecule, and large to small mutations on the right side.